이학박사 학위논문

식물 재분화와 배발생 과정에서의 DNA 메틸레이션 다이나믹스

DNA methylation dynamics

during plant regeneration and embryogenesis

2025년 2월

서울대학교 대학원

생명과학부

이 승 아

식물 재분화와 배발생 과정에서의 DNA 메틸레이션 다이나믹스

지도 교수 최 연 희

이 논문을 이학박사 학위논문으로 제출함
2025년 1월

서울대학교 대학원
생명과학부
이 승 아

이승아의 이학박사 학위논문을 인준함
2024년 12월

위 원 장 조 형 택 (인)

부위원장 최 연 희 (인)

위 원 이 병 하 (인)

위 원 현 유 봉 (인)

위 원 서 필 준 (인)

DNA methylation dynamics during plant regeneration and embryogenesis

Under the supervision of
Professor. Yeonhee Choi, Ph.D.

Submitting a Ph.D. Dissertation of
Biological Sciences
January 2025

Graduate School of Biological Sciences
Seoul National University
Biological Sciences Major
Seunga Lee

Confirming the Ph.D. Dissertation written by
Seunga Lee
December 2024

Chair	Hyung-Taeg Cho	(Seal)
Vice Chair	Yeonhee Choi	(Seal)
Examiner	Byeong-ha Lee	(Seal)
Examiner	Youbong Hyun	(Seal)
Examiner	Pil Joon Seo	(Seal)

Abstract

DNA methylation dynamics during plant regeneration and embryogenesis

Seunga Lee

School of Biological Sciences

The Graduate School

Seoul National University

Plant regeneration and embryogenesis share a fundamental reliance on dynamic epigenetic reprogramming, particularly through DNA methylation. This study employs whole-genome bisulfite sequencing (WGBS), RNA sequencing, and small RNA (sRNA) profiling to elucidate the intricate epigenetic dynamics underlying these processes in *Arabidopsis thaliana*. Plant regeneration involves significant reprogramming of DNA methylation patterns as

differentiated leaf tissues transition into pluripotent calli, eventually leading to shoot formation. During callus formation, pericentromeric transposable element (TE) regions undergo hypomethylation, predominantly in the CHH context (where H represents A, T, or C) and to a lesser degree in CG, while genic regions exhibit CG methylation redistribution enabling cellular reprogramming. The subsequent shoot regeneration phase is marked by widespread methylation across all cytosine contexts in pericentromeric TEs and dynamic CG methylation shifts in genic regions. These epigenetic alterations are critically regulated by the DEMETER (DME) DNA demethylase, which interacts with ROS1 and RNA-directed DNA methylation (RdDM) pathways to maintain methylation balance. DME mutation leads to altered methylation patterns and enhanced callus and shoot regeneration, highlighting its role as an epigenetic safeguard against TE activation and genomic instability during in vitro regeneration. During embryogenesis, CHH methylation levels gradually increase through a conserved mechanism observed across dicotyledonous plants, involving both RdDM and RNA-independent CHROMOMETHYLASE 2 (CMT2) pathways. This process features two developmental waves of sRNA accumulation from TEs, driving the coordinated expansion of CHH-methylated regions and sRNA clusters. CHH Methylation spreads through both sRNA-dependent lengthening of consecutively methylated loci and sRNA-independent mechanisms, particularly in centromeric regions. These findings underscore conserved principles of DNA methylation dynamics in regulating developmental plasticity and genomic stability. While plant

CG methylation remains relatively stable, the observed CHH methylation resetting during both plant regeneration and embryonic development mirrors mammalian CG methylation dynamics during embryogenesis. This comparative analysis provides critical insights into context-specific epigenetic strategies governing cell fate transitions, offering a framework for manipulating plant regeneration efficiency and understanding evolutionary conservation of epigenetic regulation. Collectively, this study advances our understanding of plant developmental biology and has potential implications for crop improvement, such as enhancing tissue culture techniques for plant breeding and developing strategies to maintain genomic stability during biotechnological manipulations.

Keyword: DNA methylation, Epigenetics, Plant regeneration, Embryogenesis, DEMETER, *Arabidopsis thaliana*

Student Number: 2017-28950

Table of Contents

Chapter 2. DNA methylation dynamics and CHH methylation spreading during *Arabidopsis* embryogenesis

List of Figures

List of Table

Abbreviation

RdDM	RNA-directed DNA methylation
DME	DEMETER
CMT2	CHROMOMETHYLASE 2
CIM	Callus-inducing medium
SIM	Shoot-inducing medium
RIM	Root-inducing medium
TE	Transposable element
WT	Wild type
MS	Murashige and Skoog
DAG	Days after germination
DAC	Days after CIM incubation
WGBS	Whole genome bisulfite sequencing
DMR	Differentially methylated region
DAS	Days after SIM incubation
IGR	Intergenic region
TPM	Transcripts per million
DEG	differentially expressed gene
GO	Gene ontology
GL	Globular stage embryo
H	Heart stage embryo
T	Torpedo stage embryo
BT	Bending torpedo stage embryo
MG	Mature green stage embryo
sRNA	Small RNA
sRC	sRNA clusters
meC region	Region with consecutive methylated cytosines

Chapter 1. DNA methylation dynamics and effect of DEMETER DNA demethylase during *Arabidopsis* regeneration

1.1. Introduction

Somatic cells in plants possess a distinctive capacity for dedifferentiation, enabling the induction of *de novo* organs. This remarkable property has been a cornerstone of *in vitro* tissue culture techniques. On auxin-rich callus-inducing medium (CIM), tissue explants form a pluripotent callus, which differentiates into *de novo* shoots upon transfer to shoot-inducing medium (SIM) (Figure 1) (Skoog & Miller, 1957). During callus formation, pericycle-like cells serve as the origin, with root founder cells proliferating to generate a cell mass resembling lateral root primordia on CIM (Atta et al., 2009; Sugimoto et al., 2010). The establishment of root founder cells relies on key transcription factors, WUSCHEL-RELATED HOMEOBOX11 (WOX11) and WOX12 (Liu et al., 2014), which interact with AUXIN RESPONSE FACTOR7 (ARF7) and ARF19 (Okushima et al., 2007) to activate LATERAL ORGAN BOUNDARIES DOMAINs (LBDs) (Fan et al., 2012; Feng et al., 2012), thereby promoting callus initiation and proliferation. Root stem cell regulators such as PLETHORAs (PLTs), SCARECROW (SCR), and WOX5 (Kareem et al., 2015; Kim et al., 2018; Sugimoto et al., 2010) play critical roles in establishing regenerative competence within the callus. Upon acquiring pluripotency, incubation of the callus on SIM facilitates *de novo* shoot regeneration. Cytokinin signaling mediated by Type-B

ARABIDOPSIS RESPONSE REGULATORs (ARRs) activates WUSCHEL (WUS), a key regulator involved in shoot meristem formation (Meng et al., 2017; Zhang et al., 2017).

In both plants and vertebrates, cytosine methylation functions as a vital epigenetic modification that contributes to the silencing of transposable elements (TEs), the maintenance of genome stability, and the regulation of gene expression (Jeddeloh et al., 1998; Law & Jacobsen, 2010; Zilberman et al., 2007). Unlike mammals, plants exhibit cytosine methylation at CG sites as well as CHG and CHH sites, although CG methylation remains predominant (Law & Jacobsen, 2010). In *Arabidopsis thaliana*, *de novo* DNA methylation is catalyzed by DOMAIN REARRANGED METHYLTRANSFERASE1/2 (DRM1/2) via the small RNA-directed DNA methylation (RdDM) pathway across all cytosine contexts (Cao & Jacobsen, 2002; Matzke & Mosher, 2014). METHYLTRANSFERASE1 (MET1) is an essential enzyme maintaining CG methylation (Kankel et al., 2003), while CHROMOMETHYLASE3 (CMT3) and CMT2 are responsible for sustaining CHG and CHH methylation, respectively (Law & Jacobsen, 2010; Lindroth et al., 2001; Zemach et al., 2013).

Although DNA methylation is generally stable during cell division to ensure genomic integrity, it undergoes dynamic reprogramming, including active demethylation, during various developmental processes (Heard & Martienssen, 2014; Ibarra et al., 2012; Kim et al., 2019; Park et al., 2016; Sasaki & Matsui, 2008; Schoft et al., 2011; Seisenberger et al., 2013; Seki et al., 2005). In

Arabidopsis, this process is mediated by DNA glycosylase-domain proteins, including DEMETER (DME), DEMETER-LIKE2 (DML2), DML3, and REPRESSOR OF SILENCING1 (ROS1), through the base excision repair pathway (Gehring et al., 2006; Ortega-Galisteo et al., 2008; Penterman et al., 2007). While the *ros1;dml2;dml3* triple mutants develop relatively normally, the loss of DME function results in severe developmental defects, including seed abortion and stunted growth (Choi et al., 2002; Kim et al., 2021). This suggests that DME's activity is essential for both reproductive and vegetative development, though its roles during somatic growth remain incompletely characterized.

While previous studies have identified changes in DNA methylation during plant regeneration (Chakrabarty et al., 2003; Grzybkowska et al., 2018; Shim, Lee, Park, et al., 2021; Stroud, Ding, et al., 2013), the complete landscape and molecular mechanisms underlying DNA methylation dynamics throughout the tissue culture process remain unclear. This research characterizes DNA methylation and transcriptomic dynamics in wild type Ler and *dme-2* mutants during two-step regeneration. The results suggest that the DME demethylase contributes to non-CG methylation maintenance in pericentromeric regions through the enhancement of RdDM activity during regeneration. This underscores the interaction between DME-driven demethylation and RdDM, providing valuable insights into the epigenetic reconfiguration underlying DNA methylation dynamics required for somatic cell reprogramming.

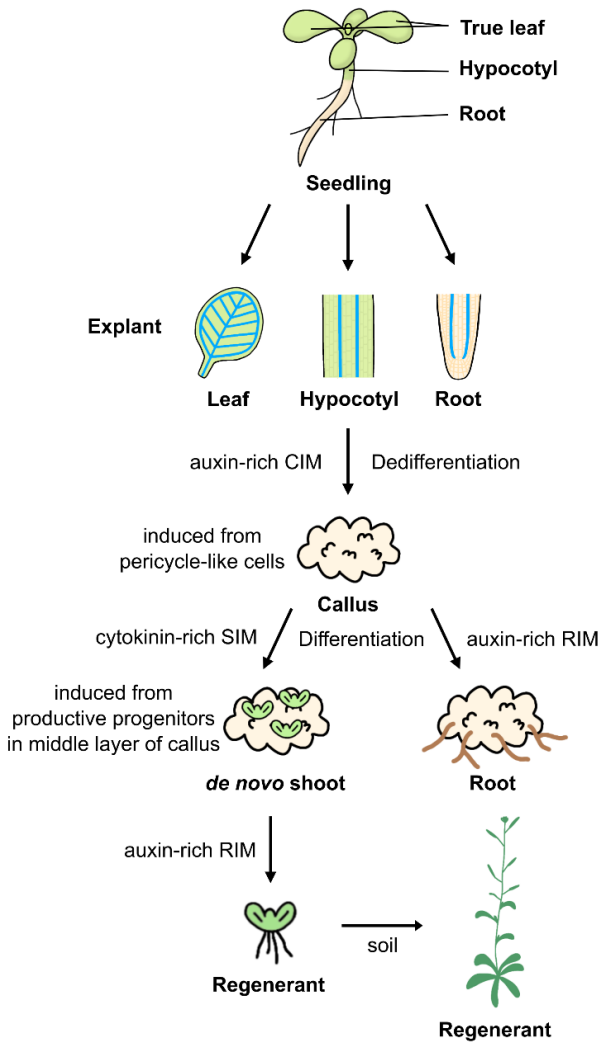

Figure 1. Overview of *in vitro* plant regeneration process.

Various plant tissues, including true leaf, hypocotyl, and root, can serve as explants for callus formation. Explants cultured on auxin-rich callus-inducing medium (CIM) undergo dedifferentiation, forming callus from pericycle-like cells. Transferring the callus to cytokinin-rich shoot-inducing medium (SIM) or auxin-rich root-inducing medium (RIM) drives differentiation, forming *de novo* shoots or roots. Notably, *de novo* shoots arise from progenitor cells in the middle layer of callus. The regeneration process involves sequential culturing on CIM, SIM, and RIM to achieve fully developed regenerants.

1.2. Material and methods

1.2.1. Plant materials and growth conditions

In this study, the Ler ecotype of *Arabidopsis thaliana* wild type (WT) and the *dme-2* mutant were used. After germination on Murashige and Skoog (MS) medium (Murashige & Skoog, 1962), the plants were cultivated in an environmentally regulated growth room with long-day conditions consisting of a 16-hour light/8-hour dark cycle. The growth room was maintained at a constant temperature of 22°C under cool white fluorescent lights at an intensity of 100 μmol/m²/s.

1.2.2. Two-step plant regeneration

For callus induction, true leaves were collected from seedlings at 14 days after germination (DAG14) to serve as explants. Calli were induced on CIM, which was composed of MS medium containing 0.5 μg/ml 2,4-dichlorophenoxyacetic acid (2,4-D) and 0.05 μg/ml kinetin. The induction process was conducted at 22°C under continuous dark conditions for 7 days. After 7 days of callus induction (DAC7), the calli were transferred to a SIM, which consisted of MS medium containing 0.9 μmol/l 3-indoleacetic acid and 2.5 μmol/l 2-isopentenyl adenine. The calli were then incubated on SIM for up to two weeks at 22°C under long-day conditions to promote *de novo* shoot formation.

1.2.3. Sample preparation for WGBS and transcriptome analysis

All samples were flash-frozen in liquid nitrogen and stored at -80°C until further processing. For whole-genome bisulfite sequencing (WGBS), four biological replicates each of leaf explants and *de novo* shoots, and three replicates of calli were prepared. Transcriptomic analyses were conducted using three biological replicates for each sample type. DNA extraction was performed following the protocol described by (Allen et al., 2006). The DNA methylome libraries were prepared using the Pico Methyl-Seq Library Prep Kit (Zymo Research, U.S.) and sequenced on the HiSeqXten platform (Macrogen, Korea). For RNA-seq, total RNA was extracted using the Qiagen RNeasy Kit (Qiagen, Germany). Libraries were prepared with the TruSeq Stranded mRNA Kit (Illumina, U.S.), and sequencing was performed on the NovaSeq 6000 platform (Macrogen, Korea).

1.2.4. WGBS data processing

From WGBS, 150 bp paired-end sequencing reads were obtained and processed using Trim Galore by removing 10 base pairs from the 5' end and 5 base pairs from the 3' end. The reads were subsequently filtered for low-quality and short reads (<40 bp) using Trimmomatic. Sequence alignment was performed using hisat2 with Bismark (option: --hisat2 --local) to map the processed reads to the *Arabidopsis* Ler reference genome (accession number GCA_900660825) (Goel et al., 2019). The Bismark toolset was then employed to remove PCR duplicates and extract methylation levels. Analysis was performed on 50 bp windowed averages, with each

window required to contain at least three cytosines and a minimum of five aligned reads. To quantify methylation levels, the number of methylated cytosines was divided by the total cytosine count at each position, with averages calculated across defined windows. The CT conversion rate was assessed using the TAIR10 plastid sequence, given that the Ler genome constructed by (Goel et al., 2019) did not include plastid genomic information.

1.2.5. Identification of DMRs

Differentially methylated regions (DMRs) were identified using the R package methylKit (Akalin et al., 2012). The average difference in methylation levels and its standard deviation were calculated for each 50 bp window. A window was identified as a DMR based on two conditions: (1) the methylation level difference was greater than one standard deviation, and (2) the corresponding q-value was less than 0.05. This approach was applied to identify both stage DMRs and *dme* DMRs.

1.2.6. RNA-Seq analysis

RNA-seq reads were aligned to the *Arabidopsis* Ler genome (accession number GCA_900660825) (Goel et al., 2019) using STAR (v2.7.10a) with the parameters "--pOverlapNbasesMin 12 --peOverlapMMp 0.1 --twopassMode Basic" (Dobin et al., 2013). Transcript abundance was quantified using RSEM (v1.3.1) (Li & Dewey, 2011). Differential gene expression analysis was performed using DESeq2 (v1.34.0), with differentially expressed genes (DEGs)

identified based on the criteria of |log2(fold-change)| > 1 and p-value < 0.05 (Love et al., 2014). Gene Ontology (GO) enrichment analysis of the DEGs was conducted using ShinyGO (v0.80) (Ge et al., 2020). For the analysis of Ler and *dme-2* seedlings, raw data were obtained from the Gene Expression Omnibus (accession number GSE164217) (Kim et al., 2021).

1.2.7. RT-qPCR

Using the QuantiTect Reverse Transcription kit (Qiagen, Germany), cDNA was synthesized following the manufacturer's protocol. Real-time quantitative PCR (RT-qPCR) was performed using the SsoAdvanced Universal SYBR Green Supermix (Bio-Rad, U.S.) with gene-specific primers (Table 1).

Table 1. Primers used in real-time qPCR for key RdDM genes.

Primer name	Sequence
ACT2-F	5’-CCTTTAACTCTCCCGCTATGT-3’
ACT2-R	5’-GTAAGGTCACGTCCAGCAAG-3’
AGO1-F	5’-TCAAGCCCATCTATTGCTGC-3’
AGO1-R	5’-ATCATGCCACCAGTCACCAC-3’
AGO4-F	5’-TGGATGGTAAAGAGTTTGCT-3’
AGO4-R	5’-CCATCACTTGGACTTTCATT-3’
NRPD2-F	5’-GATGCTAGATATCCGCACCCC-3’
NRPD2-R	5’-CAGCTCTTCCATTCCACAAGC-3’
DRM1-F	5’-TAGAGCAATTGAAGAAACCGC-3’
DRM1-R	5’-CATTCGTGATCTCTCCCACATCT-3’
DRM2-F	5’-AAAATGTGGATATTGCAGAG-3’
DRM2-R	5’-TCCTATCATTGGATTTGGTA-3’
NRPE1-F	5’-CATCCGTCTGCGTACCCTG-3’
NRPE1-R	5’-TCAACCGTGATGAAGTCAACG-3’

1.3. Results

1.3.1. Dynamics of global DNA methylation during the two-step regeneration process

WGBS was conducted on leaf explants, DAC7 calli, and DAS14 regenerated shoots to examine the dynamics of DNA methylation throughout the regeneration process (Figure 2). Average DNA methylation levels were calculated for wild type samples using probes across the whole genome, as well as those corresponding to genes or TEs separately (Figure 3). The average levels of CG methylation maintained stable patterns across the regeneration process in both genes and TEs (Figure 3A-C). In contrast, CHG methylation levels exhibited a gradual increase over the process of regeneration, with a more pronounced elevation observed in TEs during both callus formation and shoot regeneration (Figure 3D-F). CHH methylation dynamics exhibited a distinctive pattern, notably in TEs, throughout the regeneration process (Figure 3G-I). Initially, a progressive reduction in CHH methylation levels was observed during the callus formation phase. Subsequently, this trend reversed, with CHH methylation levels increasing in *de novo* regenerated shoots. This biphasic pattern of CHH methylation in TEs during two-step plant regeneration bears a striking resemblance to the methylation dynamics observed during embryogenesis. Early-stage embryos exhibit characteristically low CHH methylation levels, which progressively increase as development proceeds toward maturation (Bouyer et al., 2017; Kawakatsu et al., 2017; Lee et al., 2023; Lin et

al., 2017; Papareddy et al., 2020). The parallel between these two developmental processes suggests a conserved epigenetic mechanism governing cellular reprogramming and differentiation in plants. These findings provide insights into the epigenetic mechanisms underlying somatic cell reprogramming and plant regeneration.

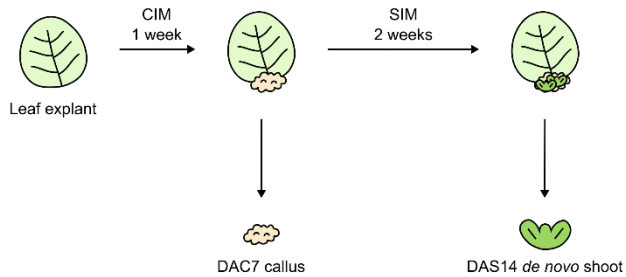

Figure 2. Two-step regeneration method applied in this study.

Leaf explants from *Arabidopsis thaliana* (Ler wild type and *dme-2* mutant) were collected 14 days post-germination (DAG14) and cultured on callus-inducing medium (CIM) for 7 days to induce callus formation. The calli were then transferred to shoot-inducing medium (SIM) to facilitate the development of *de novo* shoots. Samples used for this study included 14 DAG leaf explants, 7-day-old calli (DAC7), and 14-day-old regenerated shoots (DAS14).

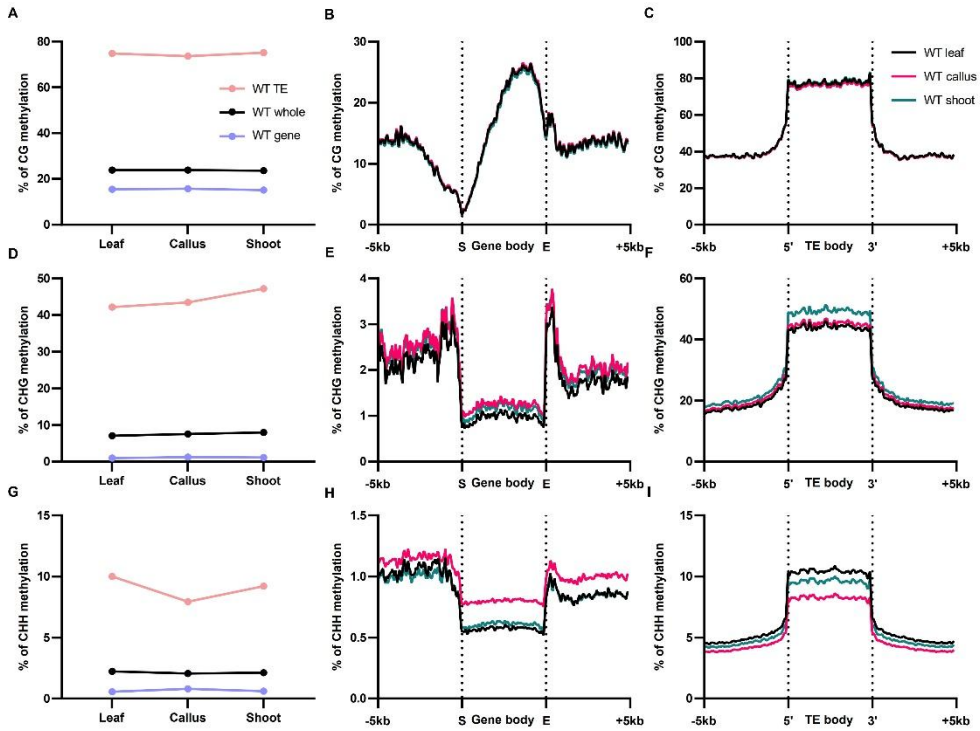

Figure 3. DNA methylation patterns across genomic features during *Arabidopsis* regeneration.

DNA methylation levels were analyzed across different genomic features throughout the regeneration process in CG (A–C), CHG (D–F), and CHH (G–I) sequence contexts. (A, D, G) Average methylation levels in whole genome, genes, and transposable elements (TEs) at leaf explant, callus, and *de novo* shoot. (B, E, H) Methylation pattern within gene bodies and their flanking regions. (C, F, I) Methylation pattern within TE bodies and their surrounding regions.

1.3.2. Considerable alterations in DNA methylation during plant regeneration

Stage-specific differentially methylated regions (DMRs) were identified to elucidate the extent and characteristics of methylation dynamics during the regeneration process. DMRs between leaf explants and callus were designated as 'c stage DMRs', while those between callus and *de novo* shoots were termed 's stage DMRs'. A considerable number of both CG c hyper DMRs (21,592) and c hypo DMRs (26,659) were observed during the leaf-to-callus transition (Figure 4), despite relatively stable global CG methylation levels (Figure 3A). CG c hyper DMRs showed predominant enrichment in genic regions, while CG c hypo DMRs were distributed roughly equally between gene and TE regions (Figure 5A, D). CG c hyper DMRs displayed a relatively uniform distribution along the chromosomes, while CG c hypo DMRs showed a notable concentration in pericentromeric areas (Figure 6A). This pattern suggests two concurrent processes during leaf-to-callus transition: a genome-wide redistribution of CG methylation in genic regions, and a significant reduction of CG methylation in pericentromeric TEs.

Upon transfer of calli to SIM, a considerable increase in the number of CG s stage DMRs was observed (Figure 4). CG s hyper DMRs were enriched in pericentromeric TEs, while CG s hypo DMRs were predominantly located in genic regions (Figure 5A, D, and 6A). The results indicate a dynamic change in CG methylation, characterized by hypomethylation in pericentromeric TEs during callus formation and their subsequent hypermethylation during *de*

novo shoot formation, along with the establishment of CG hypomethylation in genes (Figure 7).

TEs exhibited a substantial concentration of non-CG methylation (Figure 5B-D). Both non-CG hyper and hypo DMRs displayed a notable accumulation within pericentromeric regions (Figure 6B, C). For CHG methylation, hyper DMRs were predominantly located in pericentromeric regions during shoot formation (Fig. 4, 5B, 6B). In contrast, during callus induction, CHH hypo DMRs (68,015) greatly outnumbered CHH hyper DMRs (27,738), leading to global CHH hypomethylation (Figure 3G, 4), primarily at pericentromeric TEs (Figure 5C, 6C). This implies that callus originating from differentiated leaf tissue undergoes extensive epigenetic reprogramming, particularly in CHH methylation. However, after *de novo* shoot formation, the CHH methylation dynamics were reversed (Figure 8), aligning with the observed global increase in CHH methylation levels (Figure 3G-I). During this stage, s stage DMRs exhibited a markedly higher number of CHH hyper DMRs (51,116) (Figure 4A), which were concentrated in pericentromeric TEs (Figure 5C, 6C). These findings highlight substantial genome-wide changes in the DNA methylation throughout the two-step plant regeneration process, characterized by extensive reprogramming of CHH methylation during dedifferentiation and its subsequent recovery during shoot formation.

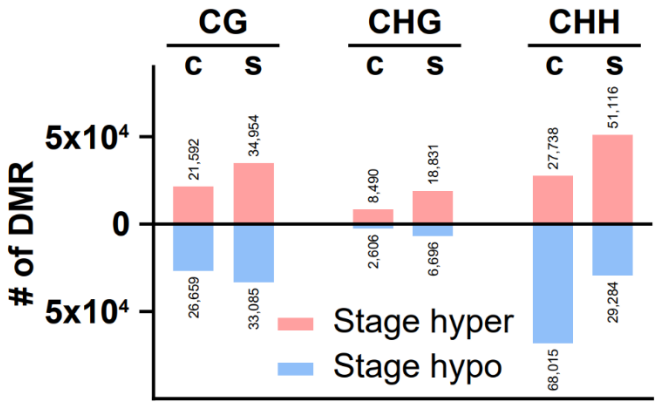

Figure 4. DMR counts of stage DMR during plant regeneration.

The total counts of stage-specific differentially methylated regions (DMRs) across CG, CHG, and CHH sequence contexts during plant regeneration are presented. DMRs between leaf explants and callus are designated as 'c stage DMRs,' while those between callus and *de novo* shoots are termed 's stage DMRs.' Red bars indicate hypermethylated DMRs (e.g., c stage hyper DMR: higher methylation in callus compared to leaf explants, or s stage hyper DMR: higher methylation in *de novo* shoots compared to callus). Blue bars represent hypomethylated DMRs (e.g., c stage hypo DMR: lower methylation in callus compared to leaf explants, or s stage hypo DMR: lower methylation in *de novo* shoots compared to callus).

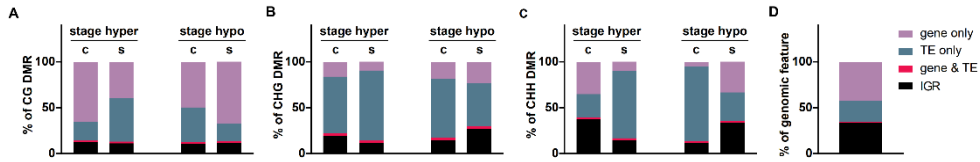

Figure 5. Genomic feature distribution of stage DMRs during plant regeneration.

(A–C) Distribution of stage DMRs across different genomic features. (D) Genomic feature composition of the reference *Arabidopsis* Ler genome shown for comparison. IGR represents intergenic regions, and "gene & TE" indicates regions where genes and transposable elements overlap.

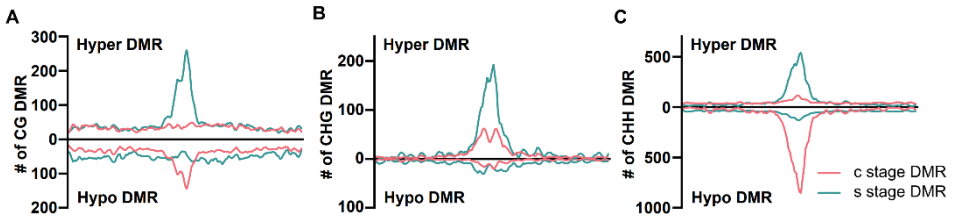

Figure 6. Chromosomal distribution of stage DMRs during plant regeneration.

Distribution of stage DMRs across CG (A), CHG (B), and CHH (C) contexts along chromosome 1 in 50 bp windows. Red lines represent c stage DMRs (leaf-to-callus transition), while green lines indicate stage DMRs (callus-to-shoot transition). For each methylation context, positive values indicate hypermethylated DMRs and negative values represent hypomethylated DMRs.

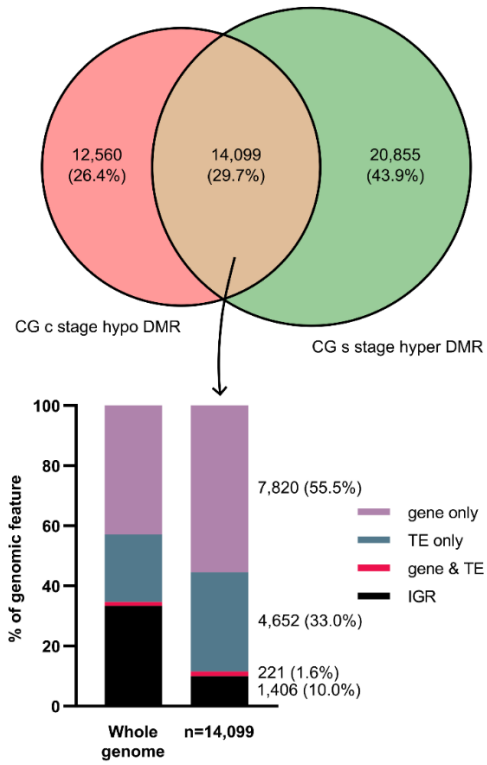

Figure 7. Genomic feature distribution of overlapping CG stage DMRs.

Venn diagram showing the overlap between CG c stage hypo DMRs (pink, 26.4%) and CG s stage hyper DMRs (green, 43.9%), with 14,099 regions (29.7%) shared between the two stages. The bar graph compares the genomic feature composition of these overlapping regions (n=14,099) to the whole genome distribution. The overlapping regions predominantly consist of genes (55.5%), followed by TEs (33.0%), IGRs (10.0%), and gene−TE overlap regions (1.6%).

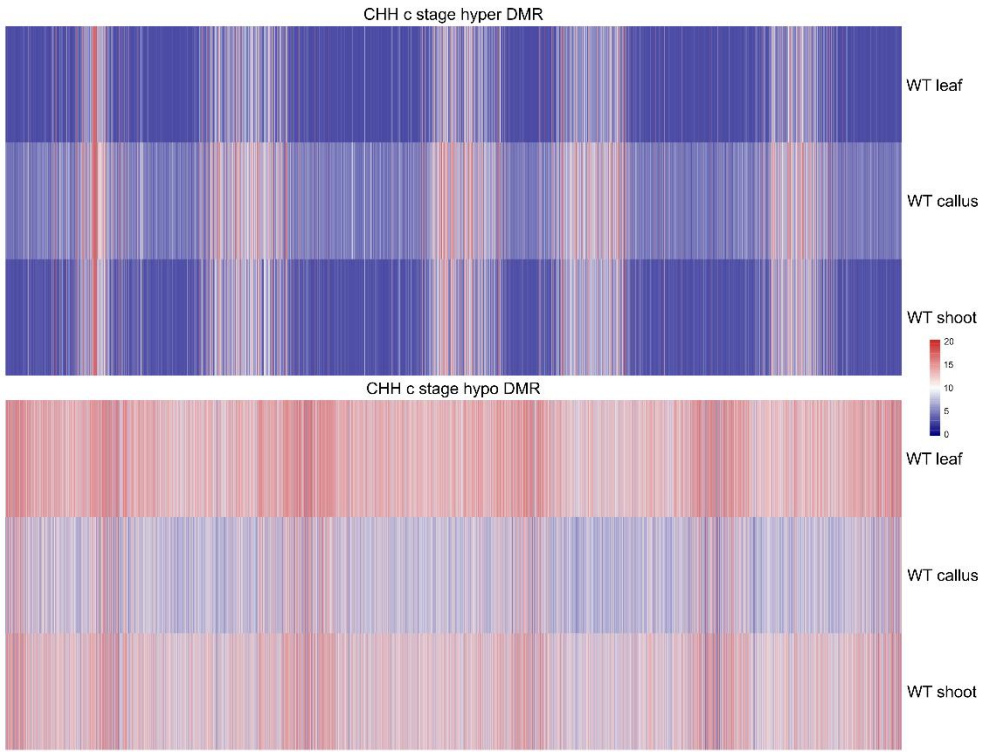

Figure 8. DNA methylation dynamics of CHH c stage DMRs during plant regeneration.

Heatmaps showing methylation levels of CHH c stage DMRs across wild type leaf explants, callus, and regenerated shoots. Upper panel represents hypermethylated DMRs and lower panel shows hypomethylated DMRs identified during the leaf-to-callus transition. Color scale indicates methylation levels from 0 (blue) to 20 (red).

1.3.3. Global hypomethylation in pericentromeric regions in *dme-2* mutant during shoot regeneration

The global methylation changes observed during wild type callus formation and shoot regeneration led us to hypothesize that active demethylation might contribute to DNA hypomethylation throughout the regeneration process. Supporting this notion, DEMETER (DME) exhibited the highest expression levels among various DNA demethylases in both DAC7 callus and DAS14 shoots (Figure 9A-B). Furthermore, *dme-2* mutants formed significantly more calli and *de novo* shoots than wild type (Kim et al., 2021), suggesting a crucial role for DME in plant regeneration.

Subsequently, genome-wide DNA methylation patterns in *dme-2* mutants were analyzed and compared to those observed in the wild type. Notably, *dme-2* mutants displayed a global reduction in methylation levels, particularly in non-CG contexts, throughout the regeneration process (Figure 10A-C, 11). This hypomethylation was strikingly apparent in the CHH context within TEs during shoot regeneration (Figure 10C). Next, the DMRs between wild type and *dme-2* mutants were analyzed at each stage. Despite similar average CG methylation levels (Figure 10A), each stage exhibited a substantial presence of CG DMRs, including both hypermethylated and hypomethylated regions. Remarkably, over 70% of these CG DMRs were located in genic regions (Figure 12, 13A, D) and showed a distribution pattern across chromosomal arms (Figure 14A). This indicates that DME plays a vital role throughout regeneration by maintaining appropriate CG methylation within genes. A significant

concentration of *dme* CG hypo DMRs in pericentromeric regions suggests a potential indirect role of the *dme-2* mutation (Figure 14A).

Unlike the gradual increase in CHG methylation levels seen during wild type regeneration, *dme-2* mutants exhibited consistently stable CHG methylation levels, which ultimately led to CHG hypomethylation (Figure 10B). This pattern was reflected in the predominance of hypo DMRs among *dme* CHG DMRs (Figure 12), which were primarily localized to pericentromeric TEs (Figure 13B, 14B). In the CHH context, wild type demonstrated a biphasic pattern of CHH methylation during regeneration, characterized by an initial decline followed by a subsequent increase. In contrast, *dme-2* mutants exhibited a continuous reduction in CHH methylation levels, leading to pronounced hypomethylation, particularly evident in *de novo* shoots (Figure 10C). Notably, a significant proportion of *dme* CHH DMRs were hypomethylated in *de novo* shoots, totaling 50,074 (Figure 12). These DMRs were predominantly derived from TEs (Figure 13C) and showed a marked accumulation in pericentromeric areas (Figure 14C).

Previous studies demonstrated that DME-driven demethylation predominantly occurs at short, AT-rich TEs located in euchromatic regions, as well as the peripheral areas of long TEs (Frost et al., 2018; Ibarra et al., 2012). Reflecting these findings, short TEs less than 500 base pairs in length were enriched in *dme* hyper CG DMRs, whereas long TEs exceeding 2000 base pairs in length were predominantly enriched in *dme* hypo DMRs across all

cytosine contexts (Figure 15). This pattern was reflected in the distribution of DMRs, with CG *dme* hyper DMRs predominantly localized to the chromosomal arms, while CG *dme* hypo DMRs showed a marked accumulation in pericentromeric areas (Figure 14A), regions where long TEs are prevalent. Collectively, these findings indicate that DME is essential not only for demethylating CG methylation in genic regions but also for maintaining methylation levels, particularly non-CG methylation and, to a smaller degree, CG methylation, within pericentromeric TEs across all three stages of the regeneration process.

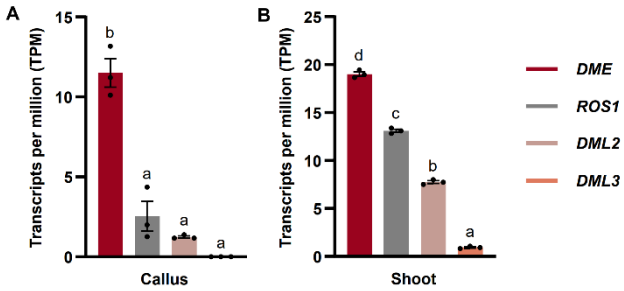

Figure 9. Expression levels of DNA demethylases in callus and *de novo* shoot.

Expression levels of DNA demethylase family genes (DME, ROS1, DML2, and DML3) in wild type callus (A) and *de novo* shoots (B) measured by RNA-seq analysis. Data are presented as transcripts per million (TPM) values with mean ± SEM from three biological replicates. Different letters above bars indicate statistically significant differences ($p < 0.05$) determined by one-way ANOVA followed by Tukey's post hoc test.

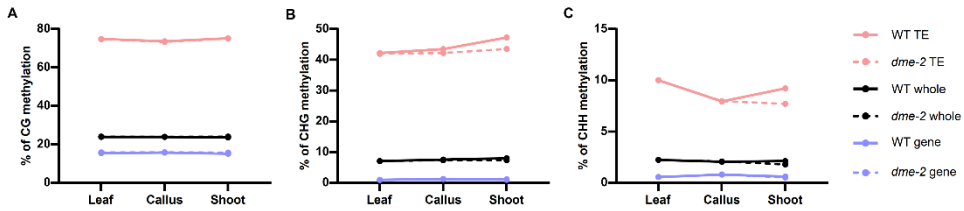

Figure 10. DNA methylation dynamics in wild type and *dme-2* mutant during plant regeneration.

Average levels of DNA methylation in Ler wild type and the *dme-2* mutant during regeneration are shown for CG (A), CHG (B), and CHH (C) contexts across different genomic features. Average DNA methylation levels in CG (A), CHG (B), and CHH (C) contexts across different genomic features during regeneration. Solid lines represent wild type (WT) and dashed lines represent *dme-2* mutant. Colors indicate different genomic features: black for whole genome, pink for TEs, and purple for genes.

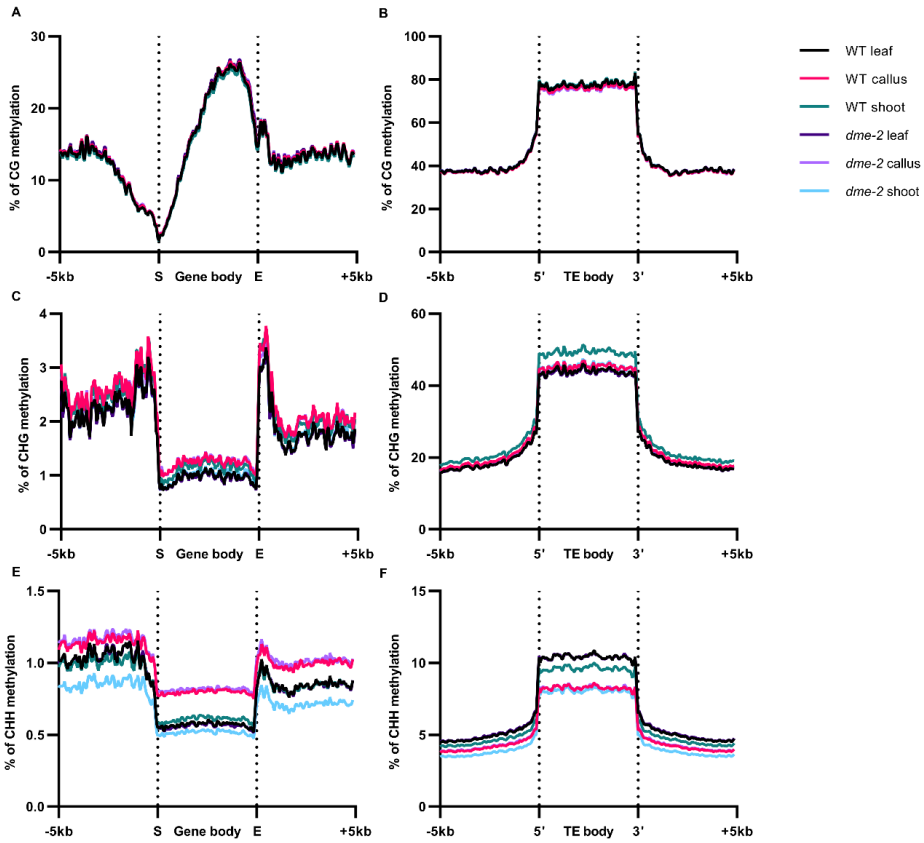

Figure 11. DNA methylation levels of genes, TEs, and their flanking regions during regeneration in WT and *dme-2* mutants.

Average DNA methylation levels in genes (A, C, E) and TEs (B, D, F) including their flanking regions (±5kb) across CG (A-B), CHG (C-D), and CHH (E-F) contexts. Vertical dotted lines mark the boundaries between gene or TE bodies and their flanking regions.

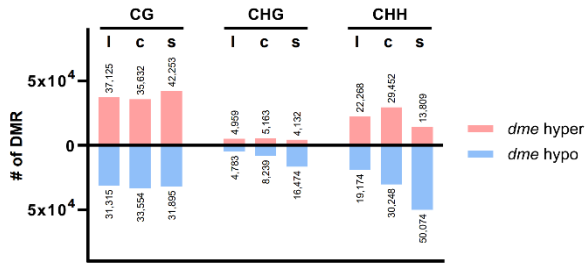

Figure 12. Stage-specific counts of *dme* DMRs during regeneration.

Total counts of differentially methylated regions (DMRs) between wild type and *dme-2* mutant across CG, CHG, and CHH sequence contexts at leaf (l), callus (c), and shoot (s) stages. Pink bars represent regions with higher methylation in *dme-2* compared to wild type (*dme* hyper DMRs), while blue bars indicate regions with lower methylation in *dme-2* (*dme* hypo DMRs).

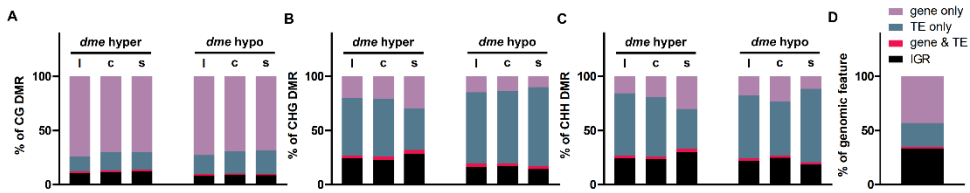

Figure 13. Genomic feature distribution of *dme* DMRs during plant regeneration.

(A–C) Distribution of *dme* DMRs across genomic features in CG (A), CHG (B), and CHH (C) contexts at leaf explant (l), callus (c), and shoot (s) stages. Stacked bars show the proportion of DMRs in different genomic features: genes (purple), TEs (blue), gene–TE overlap regions (red), and intergenic regions (IGR, black). Left panels show hypermethylated regions (*dme* hyper) and right panels show hypomethylated regions (*dme* hypo) in the *dme–2* mutant compared to wild type. (D) Genomic feature composition of the reference *Arabidopsis* Ler genome shown for comparison.

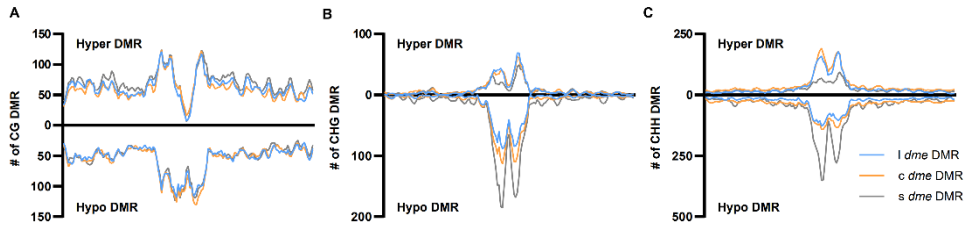

Figure 14. Genome-wide distribution of *dme* DMRs across methylation contexts during plant regeneration.

Distribution of differentially methylated regions (DMRs) between wild type and *dme-2* mutant along chromosome 1 in 50 bp windows, shown for CG (A), CHG (B), and CHH (C) contexts. Upper panels display hypermethylated regions (Hyper DMR) and lower panels show hypomethylated regions (Hypo DMR) in the *dme-2* mutant compared to wild type. Blue lines represent leaf stage (l *dme* DMR), orange lines indicate callus stage (c *dme* DMR), and gray lines show shoot stage (s *dme* DMR) DMRs. Positive values indicate higher methylation and negative values represent lower methylation in the *dme-2* mutant relative to wild type.

1.3.4. The role of DME in maintaining DNA methylation in pericentromeric regions: Potential involvement of the RdDM pathway

The observation of global hypomethylation in pericentromeric regions of *dme-2* mutants is intriguing, given DME's function as a DNA demethylase. This phenomenon could be an indirect consequence of the *dme* mutation. Given that pericentromeric non-CG methylation is regulated by both RdDM, which affects all contexts, and RNA-independent activities of CMT3 and CMT2, which primarily maintain CHG and CHH methylation respectively, expression levels of CMT3 and CMT2 were analyzed in *dme-2 de novo* shoots. The analysis revealed decreased CMT3 levels but a slight increase in CMT2 expression in the *dme-2* mutant (Figure 16) suggesting that CHH hypomethylation in *dme-2* mutants is not a result of reduced CMT2 activity. Moreover, ROS1 expression was significantly elevated in *dme-2* mutant *de novo* shoots (Figure 16), potentially explaining hypomethylation in *dme-2* (Figure 12). Interestingly, numerous key genes involved in the RdDM pathway, which were strongly upregulated during wild type *de novo* shoot regeneration (Figure 17), showed downregulation in *dme-2 de novo* shoots (Figure 18, 19). To investigate how the absence of DME affects the RdDM pathway, DNA methylation patterns were analyzed at the SDC (SUPPRESSOR OF drm1 drm2 cmt3) locus, a well-established marker for RdDM activity. The DNA methylation patterns in CG, CHG, and CHH contexts were analyzed over a 5-kb region flanking the SDC locus (Figure 20). When comparing the same tissue types between WT and *dme* mutant, significant reductions in DNA

methylation levels were observed in the *dme* mutant, particularly in non-CG contexts within the tandem repeat region. These align with previous findings that attribute the resetting of non-CG methylation in pericentromeric TE regions during wild type shoot formation, at least partially, to the RdDM pathway (Gutzat et al., 2020). Given that CHH reconfiguration is a hallmark of the reprogrammed state, the reduced CHH methylation levels in pericentromeric regions of *dme-2* shoots might indicate enhanced cellular competence for cell fate transitions (Figure 21). Collectively, these findings suggest a potential role for DME-activated RdDM in the global reestablishment of DNA methylation, with a particular emphasis on non-CG methylation, throughout the process of shoot regeneration.

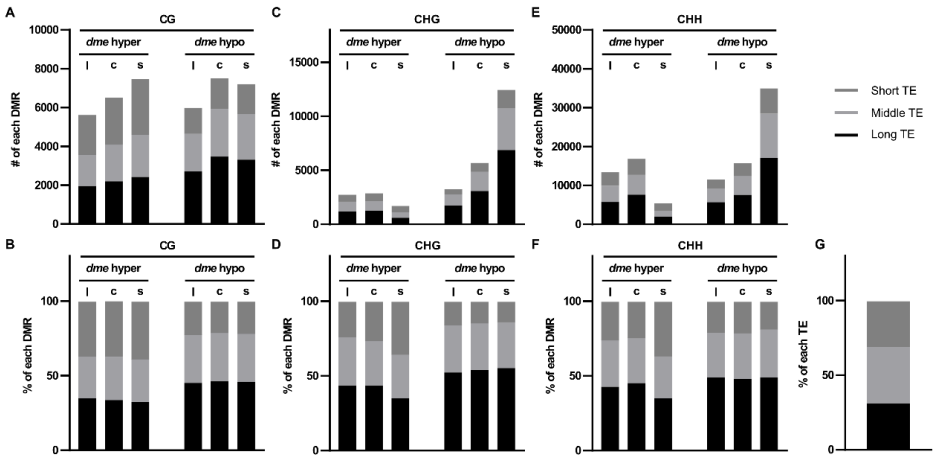

Figure 15. Classification of *dme* DMRs based on TE length.

TEs were categorized by length: short TEs (<500 bp), middle TEs (500–2000 bp), and long TEs (>2000 bp). The number of *dme* DMRs associated with each TE length category was counted (A, C, E), and their proportions were calculated for CG (B), CHG (D), and CHH (F) methylation contexts. (G) As a reference, the proportions of short, middle, and long TEs were calculated for all TEs in the *Arabidopsis* genome.

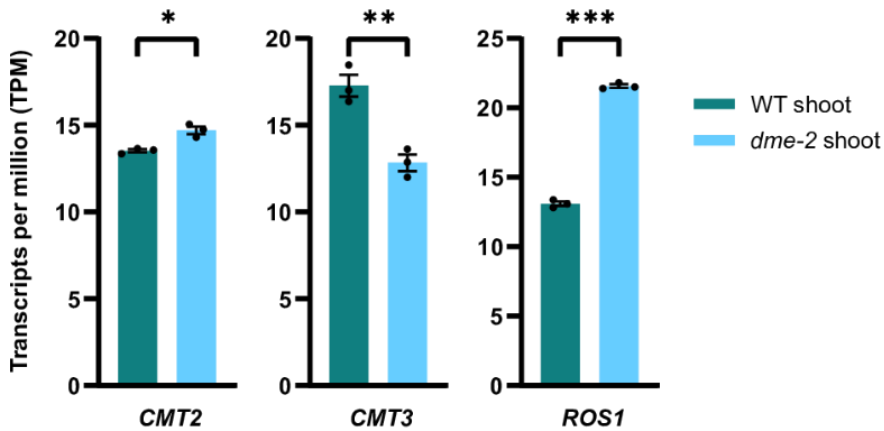

Figure 16. Expression levels of genes involved in DNA methylation in wild type and *dme-2* mutant shoots.

Expression levels of DNA methyltransferases (CMT2 and CMT3) and DNA demethylase (ROS1) genes in *de novo* shoots of wild type (dark green) and *dme-2* mutant (light blue) plants. Data are presented as transcripts per million (TPM) with mean ± SEM from three biological replicates. Statistical analysis using DESeq2 revealed significant differences between wild type and *dme-2* mutant (*p-value < 0.05, **p-value < 0.01, ***p-value < 0.001).

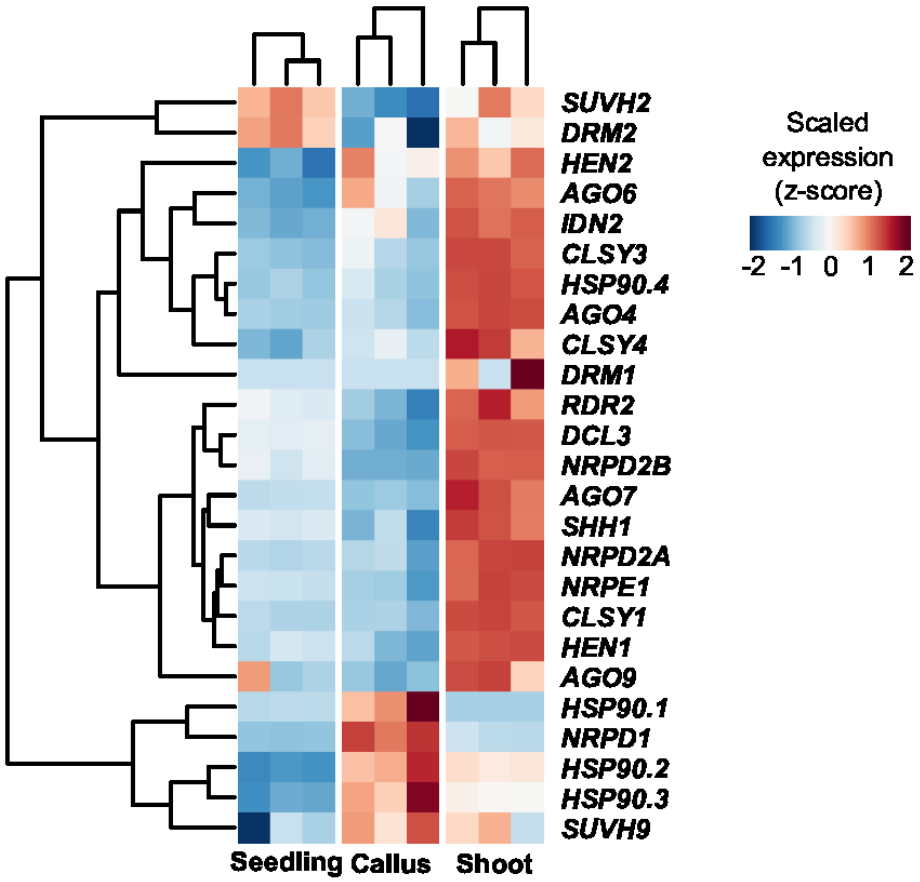

Figure 17. Expression dynamics of RdDM pathway genes during plant regeneration.

Hierarchical clustering heatmap showing expression patterns of RdDM pathway-related genes across three developmental stages: seedling, callus, and *de novo* shoot. Expression values are shown as scaled TPM (z-score) from RNA-seq data, with blue indicating lower expression (-2) and red indicating higher expression (2). The dendrogram on the left represents the hierarchical clustering of genes based on their expression patterns. RdDM components include DNA methyltransferases (DRM1, DRM2), scaffold RNA-related genes (CLSY1-4), argonaute proteins (AGO4, AGO6, AGO7, AGO9), and other pathway components (NRPD1, NRPD2A/B, NRPE1, HEN1/2, SHH1, DCL3, RDR2, SUVH2/9, HSP90.1-4, IDN2).

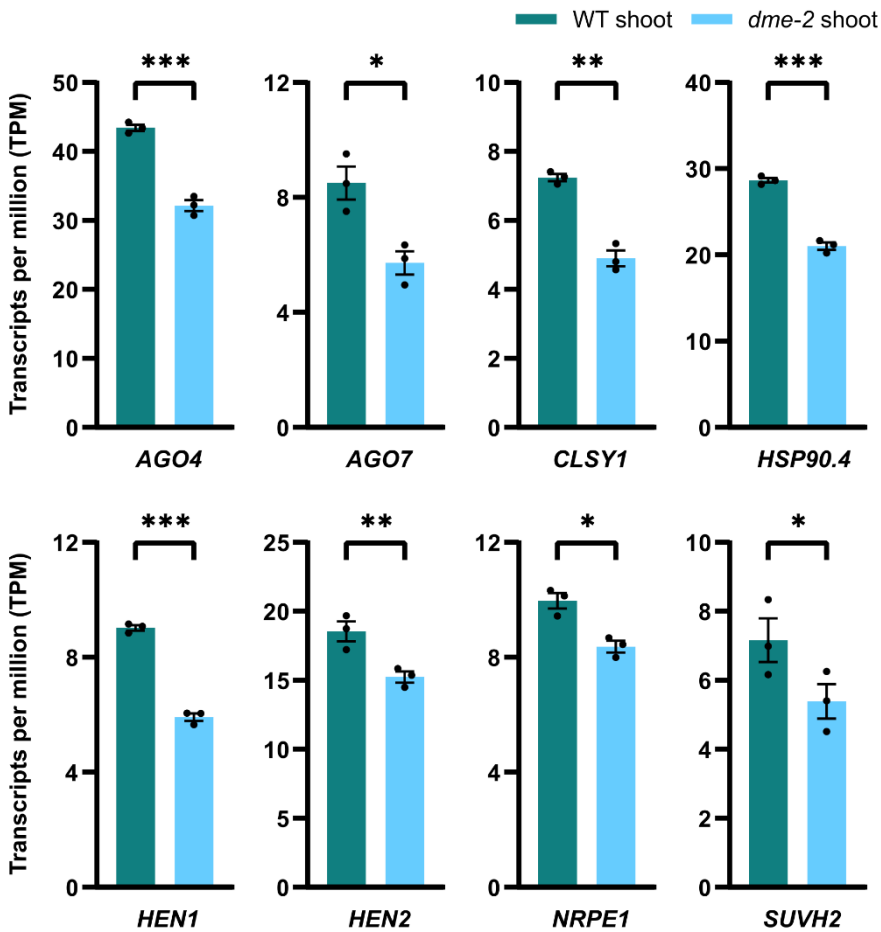

Figure 18. Expression levels of RdDM pathway genes in wild type and *dme−2* mutant *de novo* shoots.

Expression levels of RdDM pathway components in *de novo* shoots of wild type (dark green) and *dme−2* mutant (light blue) plants. Bar graphs show transcript levels (TPM) for key RdDM genes. Data are presented as mean ± SEM from three biological replicates. Statistical significance between wild type and *dme−2* mutant was determined using DESeq2 (*p−value < 0.05, **p−value < 0.01, ***p−value < 0.001).

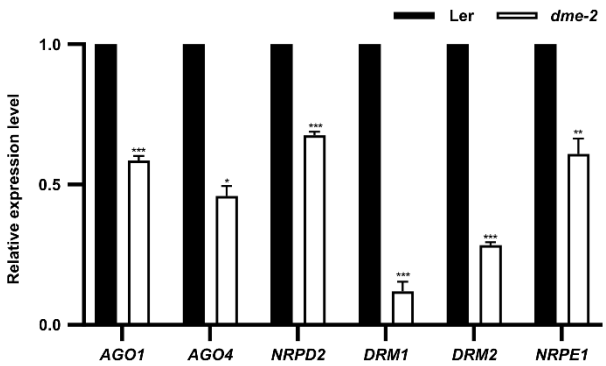

Figure 19. Relative expression of key RdDM-related genes in *de novo* shoots.

The expression levels of RdDM-related genes in DAS14 *de novo* shoots were measured using real-time qPCR. The vertical axis represents the relative gene expression levels (mean ± SE, n = 3) normalized to wild type levels. Statistical significance was determined using Student's t-test (*p-value < 0.05, **p-value < 0.01, ***p-value < 0.001).

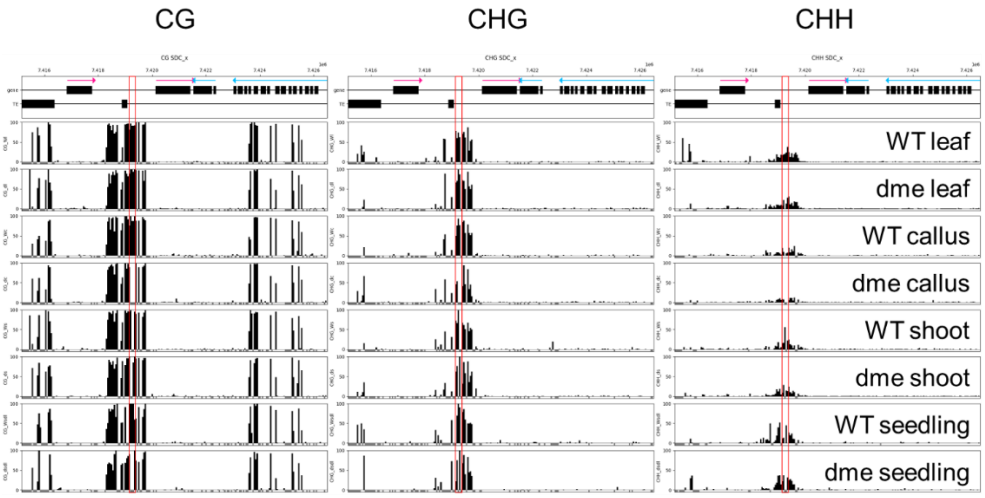

Figure 20. DNA methylation profiles at the SDC locus during plant regeneration.

Genome browser tracks showing DNA methylation levels at the SDC locus across CG, CHG, and CHH contexts in wild type and *dme-2* mutant samples. Gene structure is shown at the top of each panel, with black boxes representing exons and lines representing introns. Red boxes highlight the tandem repeat regions within the SDC locus. Methylation patterns are displayed for leaf explants, callus, *de novo* shoots, and seedlings, with wild type (WT) and *dme-2* mutant samples shown as paired tracks. Vertical scale bars represent methylation levels from 0 to 100%.

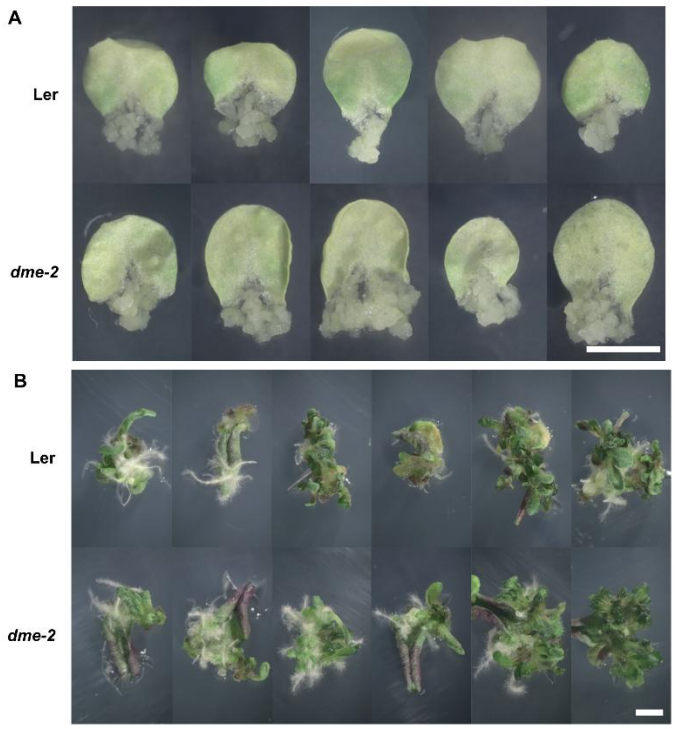

Figure 21. Phenotypic comparison of regeneration capacity between wild type and *dme-2* mutant.

(A) Callus formation from leaf explants after 14 days of culture on callus induction medium (CIM). (B) *De novo* shoot regeneration after 14 days of culture on shoot induction medium (SIM). Scale bar = 0.5 cm.

1.3.5. Misregulation of key genes driving enhanced regeneration in the *dme-2* mutant

Previous studies have demonstrated that *dme-2* mutants exhibit enhanced callus formation and shoot regeneration (Kim et al., 2021). This phenotype may be attributed to alterations in DNA methylation patterns, including localized changes affecting key DME target genes and a broader redistribution of methylation across the genome. To gain insights into the gene expression changes associated with DME-regulated plant regeneration, transcriptome analysis was performed in both wild type and *dme-2* mutant plants. Substantial transcriptional changes were observed across different stages of wild type regeneration. Comparison between original seedlings and callus identified 11,220 DEGs, while 10,748 DEGs were found between callus and *de novo* shoots. Through Gene Ontology (GO) enrichment analysis, terms such as 'callus formation' and 'lateral root development' were found to be significantly enriched in genes with increased expression during callus induction (Figure 22). In contrast, the *de novo* shoot regeneration was characterized by the activation of photosynthesis-related genes (Figure 23), accompanied by enrichment of GO terms such as "shoot system morphogenesis" and "cytokinin biosynthetic process".

The *dme-2* mutant showed notable transcriptional alterations throughout the regeneration process. Differential expression analysis identified 518 DEGs between wild type and *dme-2* calli. Further examination of the 260 genes upregulated in *dme-2* calli revealed enrichment of GO terms including "root radial pattern formation" and

"positive regulation of developmental process" (Figure 24). The enriched biological processes are likely to play a role in facilitating cellular reprogramming and inducing root-stem-like callus in *dme-2* mutants. DNA BINDING WITH ONE FINGER (DOF) transcription factor genes, including DOF2.1, HIGH CAMBIAL ACTIVITY2 (HCA2), TARGET OF MONOPTEROS6 (TMO6), and PHLOEM EARLY DOF2 (PEAR2), exhibited increased expression in *dme-2* (Figure 25). These genes are recognized as key players in tissue repair after wounding and in the process of callus formation (Zhang et al., 2022). The upregulation of these DOF genes suggests enhanced wound healing and regenerative capacity in *dme-2* mutants. Additionally, genes crucial for pluripotency acquisition, such as TRYPTOPHAN AMINOTRANSFERASE RELATED3 (TAR3) and PLETHORA5 (PLT5), also showed elevated expression in *dme-2* callus (Figure 25). PLT5, along with PLT3 and PLT7, has been implicated in establishing pluripotency and controlling regeneration in *Arabidopsis*. The upregulation of these genes is likely to contribute to the observed enhancement in callus proliferation and pluripotency in *dme-2* mutants.

The transcriptome analysis revealed a substantial increase in DEGs between wild type and *dme-2* mutants in *de novo* shoots compared to callus stage, with 1,459 DEGs identified. Genes upregulated in *dme-2 de novo* shoots exhibited enrichment of hypoxia-related GO terms (Figure 26). This enrichment suggests increased cell proliferation in *dme-2* mutants, aligning with previously observed enhanced cell division in endosperm (Choi et al.,

2002) and stomata precursor cells (Kim et al., 2021). Several key components of the cytokinin signaling pathway such as ARABIDOPSIS HISTIDINE KINASE3 (AHK3), ARR1, ARR5, ARR7, and CYTOKININ RESPONSE FACTORs (CRF6, CRF7, and CRF8) (Rashotte et al., 2006) exhibited upregulation in *dme-2 de novo* shoots (Figure 27). The increased expression of these genes indicates an enhancement of cytokinin-mediated processes in *dme-2* mutants during shoot regeneration. Additionally, Class I KNOTTED1-like homeobox (KNOXI) genes, which are crucial for stem cell maintenance and cytokinin biosynthesis, showed upregulation in *dme-2 de novo* shoots (Figure 27). These genes include SHOOT MERISTEMLESS (STM), KNOTTED-LIKE FROM ARABIDOPSIS THALIANA1 (KNAT1), KNAT2, and KNAT6 (Barton & Poethig, 1993; Gordon et al., 2007; Yanai et al., 2005). The increased expression of KNOXI genes further supports the enhanced regenerative capacity observed in *dme-2* mutants. Collectively, these transcriptional changes suggest that the *dme* mutation promotes induction of callus, acquisition of pluripotency, and formation of *de novo* shoot (Figure 21). The altered gene expression patterns observed in *dme-2* mutants are likely the result of both direct and indirect regulatory effects of DME during the plant regeneration process.

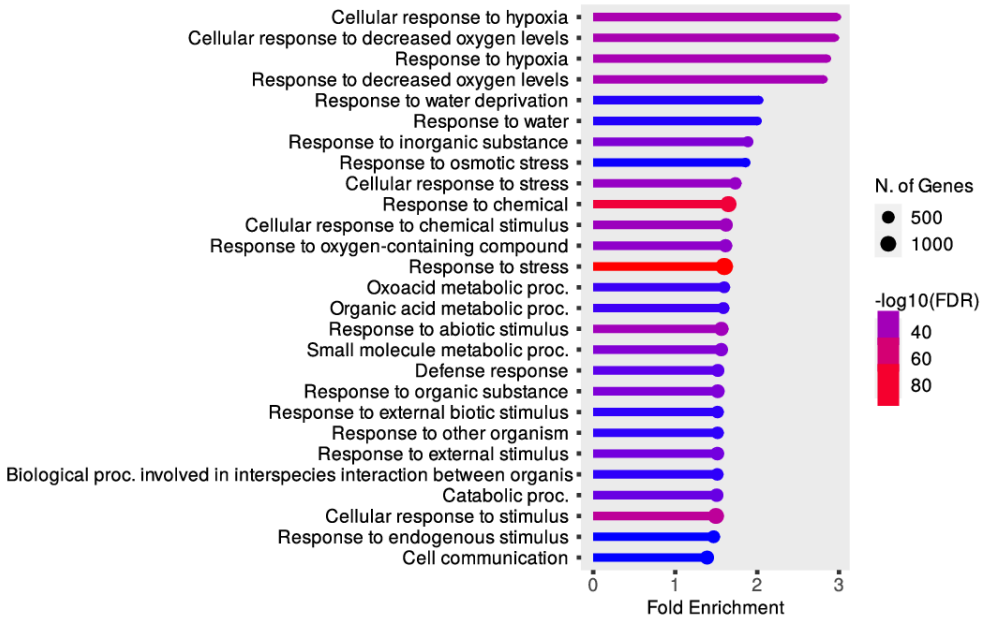

Figure 22. Gene Ontology enrichment analysis of callus-upregulated genes.

Gene Ontology (GO) biological process terms enriched in genes showing higher expression in callus compared to seedlings. The x-axis represents fold enrichment, and dot size indicates the number of genes in each category.

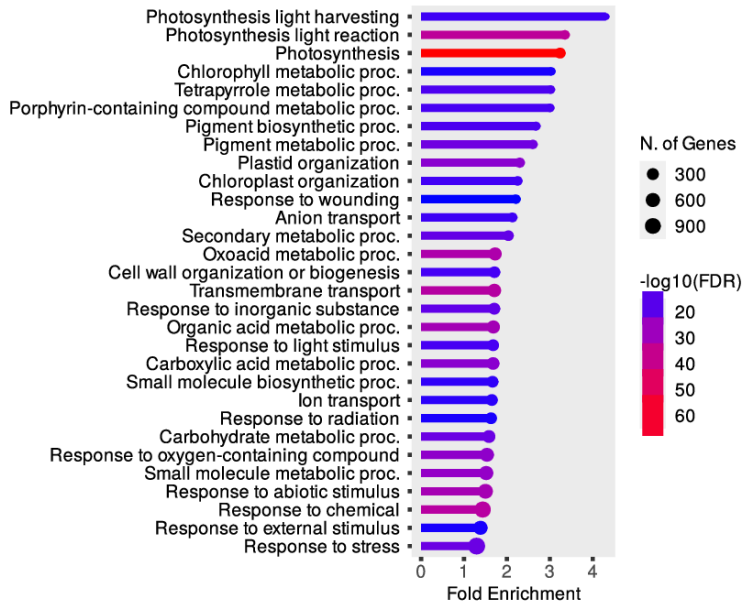

Figure 23. Gene Ontology enrichment analysis of *de novo* shoot-upregulated genes.

Gene Ontology (GO) biological process terms enriched in genes showing higher expression in *de novo* shoot compared to callus. The x-axis represents fold enrichment, and dot size indicates the number of genes in each category.

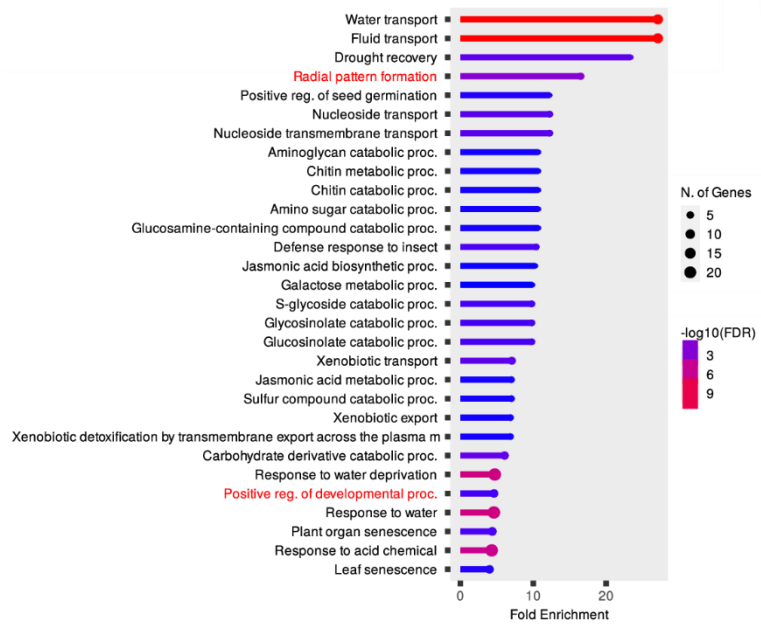

Figure 24. Gene Ontology enrichment analysis of upregulated genes in *dme-2* callus.

Gene Ontology (GO) biological process terms enriched in genes showing higher expression in *dme-2* callus compared to wild type callus. The x-axis represents fold enrichment, and dot size indicates the number of genes in each category.

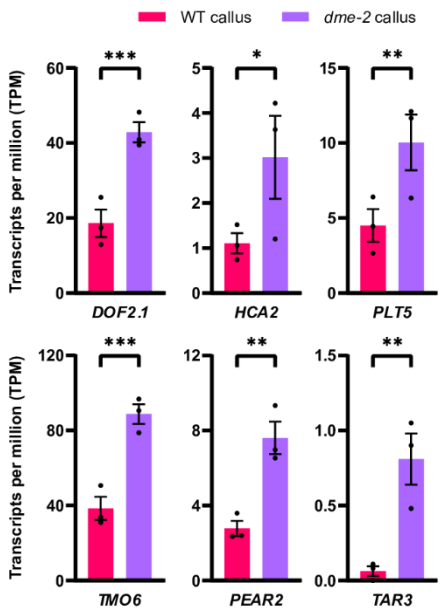

Figure 25. Expression of regeneration-associated genes in wild type and *dme-2* mutant callus.

Expression levels of key genes involved in wound-induced tissue repair, callus formation, and pluripotency acquisition in wild type (pink) and *dme-2* mutant (purple) callus tissue. Data are presented as transcripts per million (TPM) with mean ± SEM from three biological replicates. Statistical significance between wild type and *dme-2* was determined using DESeq2 (*p-value < 0.05, **p-value < 0.01, ***p-value < 0.001).

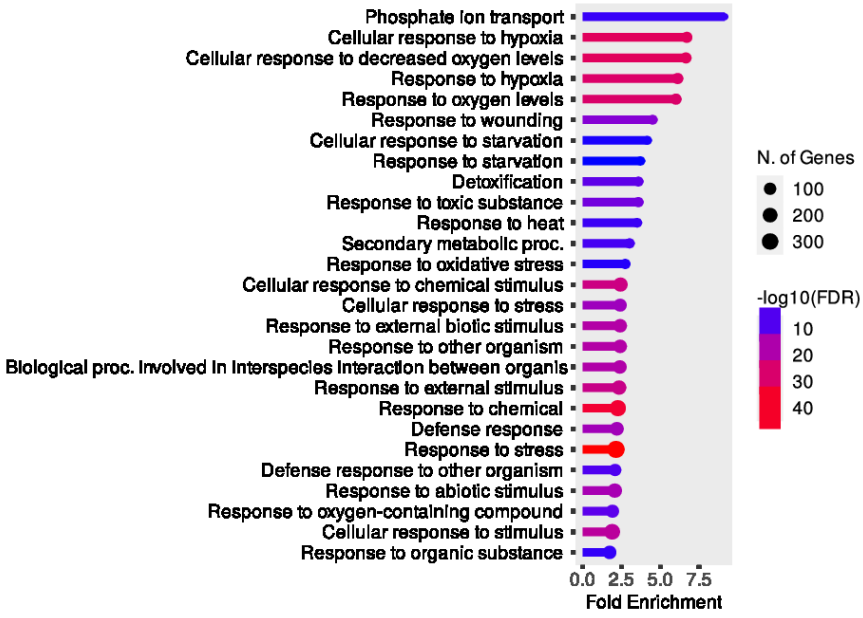

Figure 26. Gene Ontology enrichment analysis of upregulated genes in *dme-2 de novo* shoot.

Gene Ontology (GO) biological process terms enriched in genes showing higher expression in *dme-2 de novo* shoot compared to wild type *de novo* shoot. The x-axis represents fold enrichment, and dot size indicates the number of genes in each category.

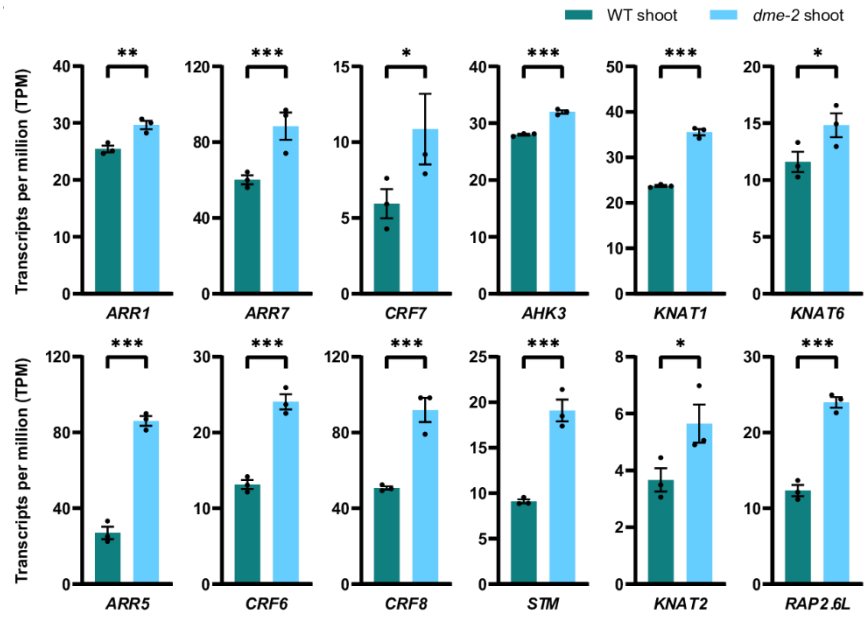

Figure 27. Expression of shoot regeneration-related genes in wild type and *dme-2* mutant *de novo* shoot.

Expression levels of genes involved in cytokinin signaling, cytokinin biosynthesis, shoot meristem regulators in wild type (dark green) and *dme-2* mutant (light blue) *de novo* shoots. Data are presented as transcripts per million (TPM) with mean ± SEM from three biological replicates. Statistical significance between wild type and *dme-2* was determined using DESeq2 (*p-value < 0.05, **p-value < 0.01, ***p-value < 0.001).

1.4. Discussion

The process of plant regeneration involves complex cellular reprogramming and tissue identity transitions, requiring dynamic changes in the epigenetic landscape, such as DNA methylation. While previous studies have suggested a connection between DNA methylation and plant regeneration (Li et al., 2011; Liu et al., 2018; Shemer et al., 2015; Shim, Lee, & Seo, 2021), the precise regulation of dynamic DNA methylation throughout the entire regeneration process remains unclear. Analysis of methylation patterns in this study confirms that pericentromeric TE regions undergo hypomethylation during callus formation, predominantly in the CHH context and to a lesser degree in the CG context. This is accompanied by a redistribution of CG methylation within genic regions, potentially playing a pivotal role in enabling the transition to a reprogrammed state. The phase of regeneration of *de novo* shoot is characterized by widespread methylation across all cytosine contexts in pericentromeric TE regions, coupled with more dynamic redistribution of CG methylation in genic regions compared to the callus formation process. These epigenetic alterations may serve as critical markers for the transition from a reprogrammed to a differentiated state.

While technical limitations have hindered the acquisition of comprehensive methylome data from egg cells, zygotes, and early embryos immediately post-fertilization, leaving the dynamics of CHH methylation somewhat speculative, the observed changes in CHH

methylation during plant regeneration exhibit parallels with the CG methylation erasure and reestablishment process in mammals, though less dramatically (Reik, 2007; Surani et al., 2007). Studies have shown that CHH methylation levels are initially low in early globular embryos and gradually increase during *Arabidopsis* embryogenesis (Bouyer et al., 2017; Kawakatsu et al., 2017; Lee et al., 2023; Lin et al., 2017; Papareddy et al., 2020). These findings suggest that plant regeneration and embryogenesis share similarities beyond phenotypic development linked to pluripotency, extending to epigenetic reprogramming. In mammals, the dynamic removal and reestablishment of CG methylation play a critical role in gamete formation and embryogenesis, leading to the hypothesis that a similar mechanism may exist in plants. However, while CG methylation levels in plants are notably higher than non-CG methylation and play a significant role in gene and TE regulation (similar to animals), they remain relatively stable. Interestingly, it is the CHH methylation levels that demonstrate a pattern of erasure and reestablishment (Bouyer et al., 2017; Kawakatsu et al., 2017; Lee et al., 2023; Lin et al., 2017; Papareddy et al., 2020), mirroring the dynamic changes observed in mammalian CG methylation. Given these observations, it is reasonable to propose that the widespread alterations in CHH methylation within pericentromeric regions could play a crucial role in epigenetic regulation during cellular fate transitions. The epigenetic reprogramming during callus formation might facilitate the acquisition of cellular competence necessary for *de novo* organogenesis. Conversely, the subsequent restoration of DNA

methylation patterns may contribute significantly to the specification and maintenance of distinct tissue identities.

The global resetting of DNA methylation during *de novo* shoot regeneration critically depends on DME function. Given DME's role as a demethylase that operates across all cytosine contexts (Gehring et al., 2006), the observation of widespread hypomethylation in pericentromeric regions of *dme-2* mutants was surprising. This phenomenon appears to stem from enhanced ROS1 demethylase activity combined with reduced efficiency of the RdDM pathway, including DRM1/2. During the regeneration process, *dme-2* mutants display more extensive pericentromeric hypomethylation compared to wild type plants, indicating a enhanced state of reprogramming. This enhanced reprogramming leads to increased callus and shoot formation, along with elevated expression of genes controlling pluripotency acquisition and shoot meristem development. Supporting these findings, drm1/2 mutants also demonstrate enhanced callus formation upon CIM induction (Jiang et al., 2015). Considering the complex interaction between ROS1 and RdDM activity plays a crucial role in maintaining appropriate DNA methylation levels (Lei et al., 2015; Williams et al., 2015), DME potentially influences ROS1-RdDM activity during sporophytic development. The elevated ROS1 expression and reduced expression of key RdDM genes in *dme* mutants support this hypothesis, although the exact molecular mechanism remains to be elucidated. Plants maintain their overall DNA methylation levels through an intricate balance between methylation and demethylation processes, regulated

by coordinated feedback mechanisms. The precise mechanisms governing the reprogramming of DNA methylation during callus formation remain unclear, though active cell proliferation and decreased small RNA populations may drive this process. Further studies are required to comprehensively unravel the molecular mechanisms underlying erasure of DNA methylation and its relationship with DME-mediated DNA methylation resetting.

Collectively, these findings highlight the critical importance of DNA methylation reprogramming in controlling cellular pluripotency and differentiation during plant regeneration. During callus formation, genome-wide hypomethylation may activate TEs, potentially triggering substantial and unexpected modifications to genome structure in *in vitro* tissue culture conditions (Miura et al., 2001). This investigation demonstrates that DME-mediated activation of the RdDM pathway serves as a crucial genetic and epigenetic safeguard, helping to maintain genome stability and prevent genomic deterioration during plant tissue culture.

Chapter 2. DNA methylation dynamics and CHH methylation spreading during *Arabidopsis* embryogenesis

2.1. Introduction

DNA methylation serves as a fundamental epigenetic mechanism that regulates various biological processes, including transcription of genes, silencing of transposon, and genomic imprinting in eukaryotic genomes. This modification is critical for proper development, as irregular DNA methylation patterns are often associated with aberrant gene expression and developmental abnormalities in both plants and vertebrates (Deniz et al., 2019; Greenberg & Bourc'his, 2019). In plants, DNA methylation occurs not only in the symmetric CG context but also in CHG and CHH contexts , in which H represents A, T, or C (Law & Jacobsen, 2010). To accommodate these distinct methylation patterns, plants have evolved a complex DNA methylation regulatory network involving diverse enzymes. One of the key pathways in this system is RNA−directed DNA methylation (RdDM) pathway, which guides DOMAINS REARRANGED METHYLTRANSFERASE 1 and 2 (DRM1/2) to its target loci, facilitating *de novo* methylation across all cytosine contexts (Cao & Jacobsen, 2002; Stroud, Ding, et al., 2013). Once *de novo* methylation established, symmetrical CG methylation is maintained by DNA METHYLTRANSFERASE 1 (MET1), while CHG methylation is preserved through CHROMOMETHYLASE 3 (CMT3)—both independently of small RNAs (sRNAs) (Law & Jacobsen, 2010). In

contrast, CHH methylation can be mediated by DRM1/2 or by CMT2, which specifically targets CHH sites within long TEs, without requiring sRNA molecules (Zemach et al., 2013).

While DNA methylation patterns are typically preserved through cell division to uphold genomic stability and cell identity, they require dynamic reprogramming during development to establish novel transcriptional profiles and define distinct cellular identities. In animals, especially mammals, DNA methylation patterns are reset each generation to erase and re-establish parental imprints (Heard & Martienssen, 2014; Sasaki & Matsui, 2008; Seisenberger et al., 2013; Seki et al., 2005). In angiosperms, central and vegetative cells, which are companion cells located adjacent to the egg and sperm respectively, undergo active DNA demethylation prior to fertilization (Ibarra et al., 2012; Kim et al., 2019; Park et al., 2016; Schoft et al., 2011). In *Arabidopsis*, methylated cytosines are specifically excised and removed by DEMETER, a DNA glycosylase, using the base excision repair (BER) pathway, thereby reprogramming the epigenome before fertilization. This epigenetic reconfiguration influences DNA methylation and gene expression profiles within the endosperm, resulting in genome-wide hypomethylation and establishment of genomic imprinting post-fertilization (Batista & Kohler, 2020; Gehring et al., 2006; Gehring & Satyaki, 2017; Ibarra et al., 2012).

While gamete companion cells and the endosperm undergo significant epigenetic reprogramming, the embryo methylome, particularly with regard to CG methylation, remains largely stable not

only throughout a single generation's development but also across generations, enabling robust transgenerational inheritance of epigenetic information (Bewick & Schmitz, 2017; Hsieh et al., 2016; Picard & Gehring, 2017). In contrast to the stability of CG methylation, CHH methylation undergoes extensive and dynamic reconfiguration following fertilization throughout embryogenesis and germination (Bouyer et al., 2017; Kawakatsu et al., 2016; Lin et al., 2017). During embryogenesis, CHH methylation levels gradually increase, and this increase in CHH methylation serves a critical function in maintaining genomic integrity by suppressing TE activity and preventing their mobilization.(Lin et al., 2017). Through a comprehensive analysis of DNA methylation dynamics and sRNA cluster during plant embryogenesis, this study provides novel insights into the developmental significance of CHH methylation and sRNA during embryogenesis.

2.2. Material and methods

2.2.1. Plant materials and growth conditions

The Col-gl ecotype of *Arabidopsis thaliana* was used in this study. The plants were grown under controlled environmental conditions with a 16-hour light/8-hour dark photoperiod at 22°C after germination on Murashige and Skoog (MS) medium. Illumination was provided by cool white fluorescent lights an intensity of 100 μmol/m²/s.

2.2.2. Embryo isolation and WGBS library construction

Fully matured wild type ovules, emasculated 24 hours prior, were fertilized with wild type pollen and incubated under standard growth room conditions until embryos reached the appropriate developmental stages for sampling. *Arabidopsis* embryos were collected at DAP4, 5, 7, 9, and 12, which represent the globular, heart, torpedo, bending torpedo, and mature green stages, respectively. Stage-specific methods were employed to isolate embryos. To isolate globular embryos, seeds were gently ground with a pestle until the embryos were released. Heart-stage embryos were obtained by making fine incisions into the seeds using tweezers. For later developmental stages, from torpedo to mature green, the seed coat and endosperm were punctured using tweezers, and the embryos were carefully pushed out afterward. Released embryos were individually collected under a microscope using microcapillaries to ensure precision. All procedures, including pollination, embryo

sampling, genomic DNA extraction, bisulfite library preparation, and whole-genome bisulfite sequencing (WGBS) data processing, followed previously established methods described in detail by (Yoo et al., 2021). All libraries were generated with at least two biological replicates, achieving high-quality metrics including robust CT conversion rates (>99%) and genome coverage exceeding 40X, meeting the recommended standards for methylome analysis (Ziller et al., 2015).

2.2.3. Global DNA methylation analysis

To analyze global DNA methylation, the embryo methylation data was segmented into 50 bp windows, each containing at least three cytosines with a minimum coverage of five reads at every developmental stage and for each cytosine context.

2.2.4. sRNA-Seq analysis

The sRNA-Seq datasets used in this study were sourced from the NCBI GEO database (GSE98553, GSE132066, GSE152971) (Lutzmayer et al., 2017; Papareddy et al., 2020; Plotnikova et al., 2019). Adapter sequences were trimmed, and quality control was performed using Trimmomatic (v0.39) and Cutadapt (v3.4), followed by the selection of reads in the 18–26 nt range. Structural non-coding RNA reads, including rRNA, tRNA, and snRNA, were filtered out by mapping pre-processed reads to the RNACentral database (v17) using bowtie (v1.3.0, parameters: -v 1 -m 0 -a). The remaining reads were aligned to the TAIR10 genome using bowtie

(v1.3.0, −v 0 −m 0 −a) and subsequently re−aligned with ShortStack (v3.8.5) under specific parameters (–align_only –mismatches 0 –mmap u –bowtie_m 1000 –ranmax 3). Reads corresponding to known microRNA precursors were excluded using Bedtools intersect (v2.30.0), and the resulting microRNA−free reads were processed for further analysis. Read clustering was performed for each sample using ShortStack with optimized parameters (–dicermin 20 –dicermax 24 –foldsize 300 –pad 1(or 75), –mincov 1.0rpmm –nohp) (Johnson et al., 2016).

2.2.5. Calculation of average length for methylated blocks

The average length of regions with consecutive methylated cytosines (meC regions) was determined for each stage of embryo development by first defining 10 bp windows containing at least one methylation site supported by five or more aligned reads. Windows with methylation levels above 5%, 10%, or 15% were merged across all stages for each cytosine context if the distance between them was less than 40 bp. The length of the resulting merged windows was averaged to characterize the size of methylated regions during each stage of embryo development.

2.2.6. Correlation between sRNA clustering and DNA methylation spreading

To investigate the relationship between CHH methylation spreading and sRNA clustering during embryonic development, meC regions in CHH context were identified if they appeared in at least three out of

five stages, with a minimum methylation level of 15%. Similarly, sRNA clusters shared across at least five out of eight stages were selected. The CHH-meC regions were then categorized into two groups based on their overlap with sRNA clusters. Finally, the average length of regions with and without sRNA clustering was calculated for comparison.

2.3. Results

2.3.1. Dynamics of global DNA methylation during embryo development

The pericentromeric regions of *Arabidopsis* chromosomes exhibit high levels of DNA methylation across all cytosine contexts, as previously observed (Cokus et al., 2008; Lister et al., 2008). This is primarily due to the enrichment of repetitive sequences and heterochromatic TEs in these regions (Figure 14B). Consistent with prior studies (Bouyer et al., 2017; Kawakatsu et al., 2017; Lin et al., 2017; Papareddy et al., 2020), CG methylation levels remained relatively stable during embryogenesis, while non-CG methylation showed significant dynamics (Figure 28, 29). Notably, global CHH methylation in pericentromeric regions gradually increased during development, reaching a peak as seeds matured (Figure 28, 29C). This increase was primarily associated with TEs, whereas methylation of genic regions remained largely unchanged across all cytosine contexts (Figure 29). CHH methylation levels in genic regions showed only minor increases, while CHG methylation in TEs exhibited a slight decline between DAP7 and DAP9 before stabilizing during later stages (Figure 29B, C).

To further investigate methylation changes during embryogenesis, genic and TE and their flanking regions were analyzed separately (Figure 29D-I). In genic regions, genome-wide methylation changes were minimal (<0.7%) across all cytosine contexts during embryo development, though distinct levels of CHG

and CHH methylation were observed at each stage (Figure 29D-F). A small yet noticeable (1%) increase in CHH methylation at the 5′ and 3′ ends of genes was apparent particularly from the globular-torpedo to the bending torpedo-mature green stages, attributable to overlapping TE sequences near gene boundaries (Figure 29F). Among the developmental stages, the torpedo stage (DAP7) exhibited the lowest CHG methylation levels (Figure 29B, E).

In TEs, a slight increase in CG methylation was observed over the course of embryogenesis (Figure 29G-I). CHH methylation, however, demonstrated a prominent, continuous increase, with a sharp rise observed between DAP5 and DAP7 (Figure 29I). Intriguingly, this increase in CHH methylation coincided with a reduction in CHG methylation during the heart-to-torpedo transition phase (Figure 29B, C, H, I). Such an inverse relationship suggests a potential interplay between CHG and CHH methylation, working in tandem to repress TEs during this critical phase, which marks the initiation of embryo maturation following pattern formation.

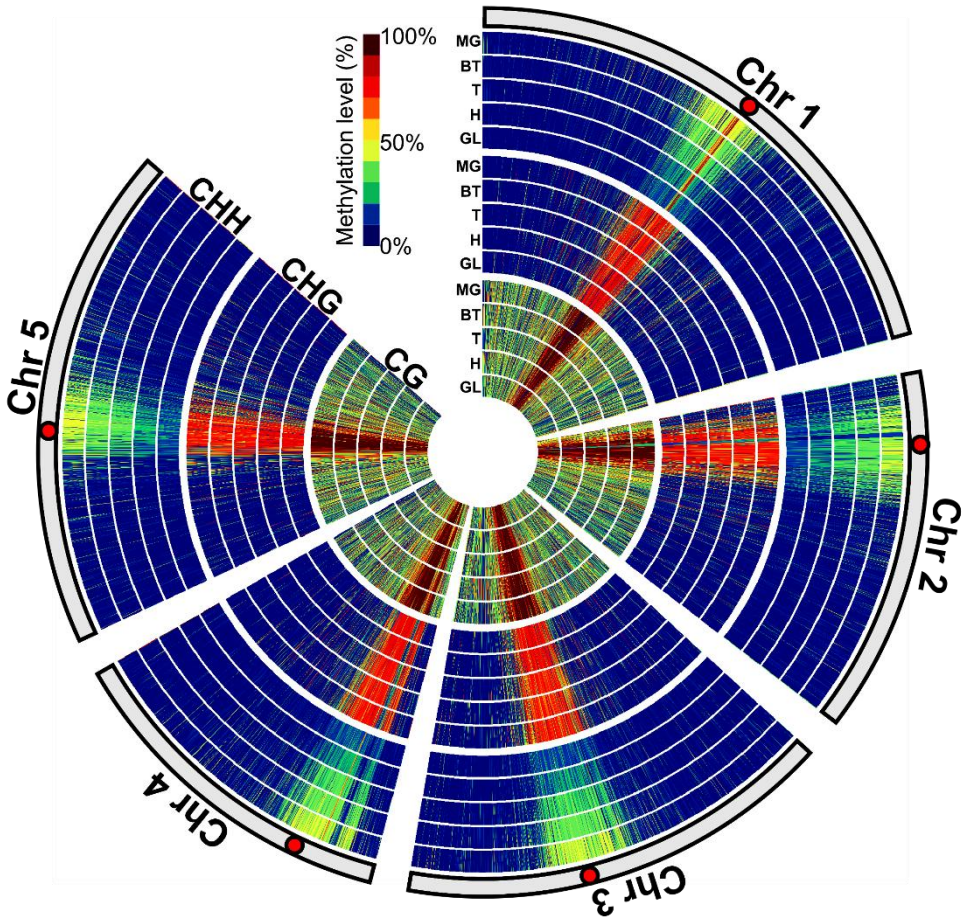

Figure 28. Genome-wide DNA methylation patterns during embryo development.

Circular heatmap showing DNA methylation levels across five *Arabidopsis* chromosomes (Chr 1-5) in CG, CHG, and CHH sequence contexts during embryo development. Concentric circles represent sequential developmental stages from inner to outer rings: globular (GL), heart (H), torpedo (T), bending torpedo (BT), and mature green (MG). Color scale indicates methylation levels from 0% (blue) to 100% (dark red). Red dots on the outer circle mark centromeric regions of each chromosome.

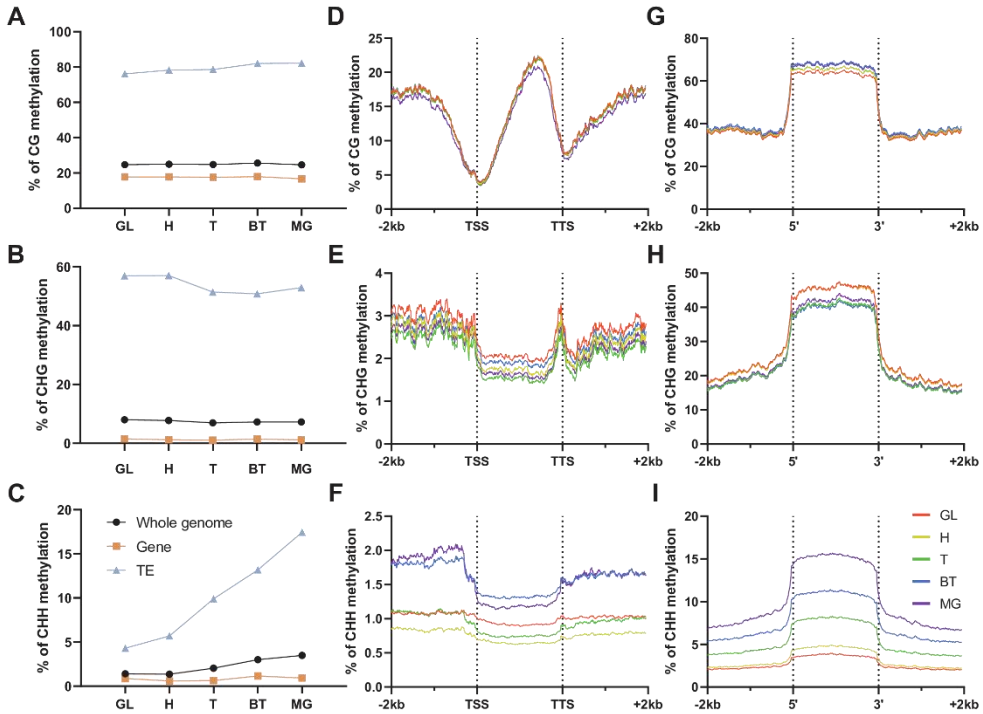

Figure 29. DNA methylation dynamics across genomic features during embryo development.

(A–C) Average DNA methylation levels in CG (A), CHG (B), and CHH (C) contexts across whole genome (black), genes (orange), and transposable elements (TEs, blue) during five embryonic stages: globular (GL), heart (H), torpedo (T), bending torpedo (BT), and mature green (MG). (D–F) Methylation profiles of genes and their flanking regions (±2kb) in CG (D), CHG (E), and CHH (F) contexts across transcription start sites (TSS) and transcription termination sites (TTS). (G–I) Methylation patterns of TEs and their flanking regions (±2kb) in CG (G), CHG (H), and CHH (I) contexts.

2.3.2. CHH methylation spreading and expansion of sRNA cluster during embryo development

De novo CG methylation spreads from cis-regulatory elements to distal CpG sites during mammalian embryogenesis (Turker, 2002). To explore whether a similar phenomenon occurs in plants during embryonic development, the average lengths of regions with consecutive methylated cytosines (meC regions) in all contexts were calculated at various developmental stages. When windows with methylation levels exceeding 5%, 10%, or 15% were merged (provided they were within 40 bp of each other), a gradual increase in the length of CHH-meC regions was observed as embryos matured (Figure 30A-C). This trend was particularly pronounced when the 15% methylation cutoff was applied (Figure 30C), indicating that CHH methylation spreads across the genome during embryogenesis.

The RdDM pathway, which mediates *de novo* DNA methylation in *Arabidopsis* (Chow et al., 2020; Erdmann & Picard, 2020; Matzke & Mosher, 2014), may play a critical role in CHH methylation spreading. However, it remains unclear whether this pathway is required only for the initial establishment of methylation during early embryogenesis or if sRNAs are continuously necessary to maintain and propagate CHH methylation in later stages. To determine whether sRNAs continuously contribute to CHH methylation spreading, the average length of 24-nt sRNA clusters was measured by merging clusters located within 75 bp of each other across developmental stages using publicly available sRNA datasets

(Papareddy et al., 2020). Results showed a progressive lengthening of sRNA clusters as embryos advanced in development (Figure 30D), suggesting that ongoing sRNA expression near methylated regions contributes to the spreading of CHH methylation to adjacent unmethylated sites.

Then, the relationship between extended sRNA expression and CHH methylation spreading was assessed by comparing the average lengths of regions where CHH-meC regions overlapped with merged 24-nt sRNA clusters. A linear increase of sRNA cluster length was observed in CHH-overlapping regions throughout development, reinforcing the positive relationship between CHH methylation spreading and sRNA activity (Figure 31A, green bars). Although CHH-meC regions without sRNA clusters also expanded during embryogenesis (Figure 31A, pink bars), these accounted for fewer loci and exhibited limited spreading. Furthermore, positional analysis revealed that such non-sRNA overlapping CHH-meC regions were concentrated in centromeric regions and were likely mediated by CMT2 (Figure 31B). Visualization of individual loci further confirmed that the extension of sRNA expression coincided with CHH methylation spreading and accumulation across development (Figure 32). These results align with previous findings that the RdDM pathway significantly contributes to CHH methylation increase during embryogenesis (Hsieh et al., 2023).

Collectively, these findings highlight the importance of the RdDM pathway in initiating *de novo* CHH methylation and promoting its expansion to nearby regions, facilitated by the continuous

expression and extension of sRNA clusters. This mechanism results in broader CHH-methylated regions and elevated methylation levels as embryogenesis progresses.

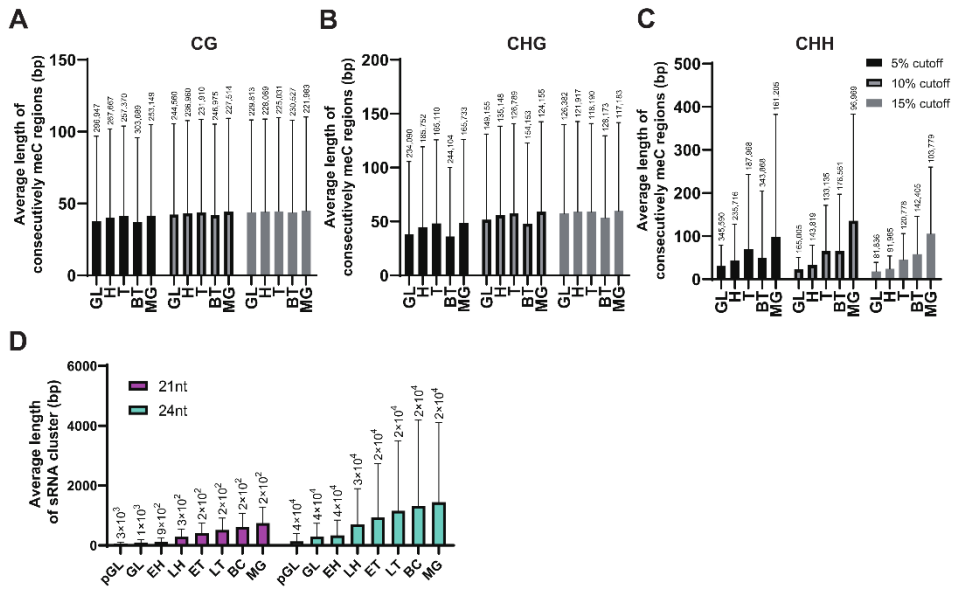

Figure 30. Length of consecutively methylated regions and sRNA clusters during embryo development.

(A–C) Average length of consecutively methylated cytosine regions (meC regions) in CG (A), CHG (B), and CHH (C) sequence contexts across embryonic stages (GL: globular, H: heart, T: torpedo, BT: bending torpedo, MG: mature green). Bar colors indicate different methylation level cutoffs. (D) Average length of sRNA clusters shown separately for 21–nt and 24–nt size classes across developmental stages (pGL: pre–globular, GL: globular, EH: early heart, LH: late heart, ET: early torpedo, LT: late torpedo, BC: bent cotyledon, MG: mature green). Whiskers represent standard deviations, and numbers above them indicate the total number of meC regions or sRNA clusters.

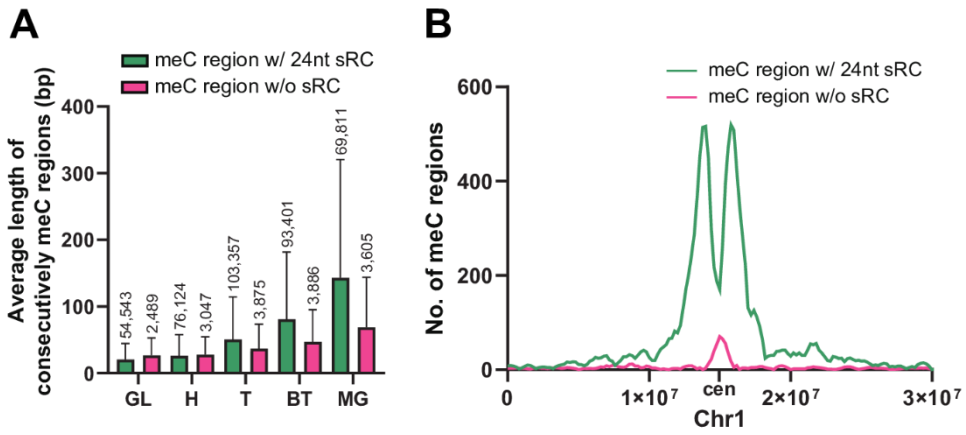

Figure 31. Average length and distribution of consecutively methylated regions on chromosome 1.

(A) Average length of consecutively methylated cytosine (meC) regions in CHH context during embryo development. Green bars represent meC regions overlapping with 24-nt small RNA clusters (sRC), while pink bars show meC regions without sRC overlap. Numbers above whiskers indicate the total count of meC regions in each category. Whiskers represent standard deviations. (B) Distribution of meC regions along chromosome 1 in 200-kb bins. Green line shows the number of meC regions overlapping with 24-nt sRC, and pink line represents meC regions without sRC overlap. The centromeric region is marked as 'cen' on chromosome 1.

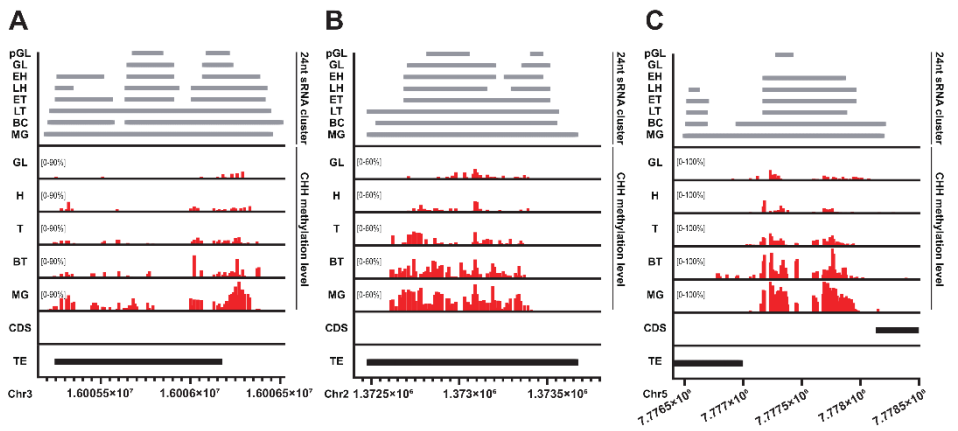

Figure 32. Representative genomic loci showing gradual CHH methylation expansion during embryo development.

Representative genomic regions showing CHH methylation patterns across developmental stages (GL: globular, H: heart, T: torpedo, BT: bending torpedo, MG: mature green). Gray bars at the top represent small RNA cluster distribution from published datasets with slightly different developmental staging (pGL: pre-globular, GL: globular, EH: early heart, LH: late heart, ET: early torpedo, LT: late torpedo, BC: bent cotyledon, MG: mature green). Red peaks represent CHH methylation levels. Black bars at the bottom show the positions of coding sequences (CDSs) and transposable elements (TEs).

2.4. Discussion

DNA methylation plays a crucial role in plant development, with distinct patterns observed across different cytosine contexts during embryogenesis. A gradual increase in CHH methylation during embryo development has been observed in multiple dicotyledonous plants, including *Arabidopsis* (Bouyer et al., 2017; Kawakatsu et al., 2017), *Brassica rapa* (Grover et al., 2020), soybean (Lin et al., 2017), and chickpea (Rajkumar et al., 2020), suggesting a fundamental and conserved role for CHH methylation in plant embryo development and genome stability.

Consistent with prior research (Bouyer et al., 2017; Kawakatsu et al., 2017; Lin et al., 2017), this study demonstrates that CHH methylation levels gradually rise during *Arabidopsis* embryogenesis, while CG and CHG methylation remain consistently high. In *Arabidopsis*, this increase is coupled at least two waves of sRNA accumulation originating from thousands of TEs (Papareddy et al., 2020). The increase in CHH methylation levels occurs through a coordinated mechanism involving two key processes: the simultaneous expansion of CHH-methylated regions to nearby loci and the coordinated expansion of sRNA clusters. This expansion mechanism is evidenced by the progressive lengthening of consecutively methylated regions and sRNA clusters as embryos advance in development. The relationship between extended sRNA expression and CHH methylation spreading is demonstrated by the linear increase in sRNA cluster length throughout development,

particularly in CHH-overlapping regions.

Notably, while CHH methylation regions without sRNA clusters also expanded during embryogenesis, these accounted for fewer loci and exhibited limited spreading, primarily concentrated in centromeric regions. Individual loci analysis confirmed that the extension of sRNA expression coincided with CHH methylation spreading and accumulation across development. This process involved not only sRNA-dependent pathways but also sRNA-independent enzymes such as CMT2, with the accumulation of sRNAs and the expression of associated enzymes were positively associated with CHH methylation resetting (Papareddy et al., 2020). These findings significantly advance our understanding of epigenetic regulation during plant embryogenesis, highlighting the complex interplay between DNA methylation and sRNAs throughout embryo development.

References

Akalin, A., Kormaksson, M., Li, S., Garrett-Bakelman, F. E., Figueroa, M. E., Melnick, A., & Mason, C. E. (2012). methylKit: a comprehensive R package for the analysis of genome-wide DNA methylation profiles. Genome Biology, 13, 1-9.

Allen, G. C., Flores-Vergara, M., Krasynanski, S., Kumar, S., & Thompson, W. (2006). A modified protocol for rapid DNA isolation from plant tissues using cetyltrimethylammonium bromide. Nature Protocols, 1(5), 2320-2325.

Atta, R., Laurens, L., Boucheron-Dubuisson, E., Guivarc' h, A., Carnero, E., Giraudat-Pautot, V., Rech, P., & Chriqui, D. (2009). Pluripotency of Arabidopsis xylem pericycle underlies shoot regeneration from root and hypocotyl explants grown in vitro. Plant J, 57.

Barton, M. K., & Poethig, R. S. (1993). Formation of the shoot apical meristem in Arabidopsis thaliana: an analysis of development in the wild type and in the shoot meristemless mutant. Development, 119(3), 823-831.

Batista, R. A., & Kohler, C. (2020). Genomic imprinting in plants-revisiting existing models. Genes Dev, 34(1-2), 24-36.

Belmonte, M. F., Kirkbride, R. C., Stone, S. L., Pelletier, J. M., Bui, A. Q., Yeung, E. C., Hashimoto, M., Fei, J., Harada, C. M., Munoz, M. D., Le, B. H., Drews, G. N., Brady, S. M., Goldberg, R. B., & Harada, J. J. (2013). Comprehensive developmental profiles of gene activity in regions and subregions of the Arabidopsis seed. Proc Natl Acad Sci U S A, 110(5), E435-444.

Bewick, A. J., & Schmitz, R. J. (2017). Gene body DNA methylation in plants. Curr Opin Plant Biol, 36, 103-110.

Bourguet, P., Picard, C. L., Yelagandula, R., Pelissier, T., Lorkovic, Z. J., Feng, S., Pouch-Pelissier, M. N., Schmucker, A., Jacobsen, S. E., Berger, F., & Mathieu, O. (2021). The histone variant H2A.W and linker histone H1 co-regulate heterochromatin accessibility and DNA methylation. Nat Commun, 12(1), 2683.

Bouyer, D., Kramdi, A., Kassam, M., Heese, M., Schnittger, A., Roudier, F., & Colot, V. (2017). DNA methylation dynamics during early plant life. Genome Biology, 18, 1-12.

Cao, X., & Jacobsen, S. E. (2002). Role of the Arabidopsis DRM methyltransferases in de novo DNA methylation and gene silencing. Current Biology, 12(13), 1138-1144.

Chakrabarty, D., Yu, K.-W., & Paek, K. Y. (2003). Detection of DNA methylation changes during somatic embryogenesis of Siberian ginseng (Eleuterococcus senticosus). Plant Science, 165(1), 61-68.

Chenais, B., Caruso, A., Hiard, S., & Casse, N. (2012). The impact of transposable elements on eukaryotic genomes: from genome size increase to genetic adaptation to stressful environments. Gene, 509(1), 7-15.

Choi, Y., Gehring, M., Johnson, L., Hannon, M., Harada, J. J., Goldberg, R. B., Jacobsen, S. E., & Fischer, R. L. (2002). DEMETER, a DNA glycosylase domain protein, is required for endosperm gene imprinting and seed viability in Arabidopsis. Cell, 110.

Chow, H. T., Chakraborty, T., & Mosher, R. A. (2020). RNA-directed DNA Methylation and sexual reproduction: expanding beyond the seed. Curr Opin Plant Biol, 54, 11-17.

Cokus, S. J., Feng, S., Zhang, X., Chen, Z., Merriman, B., Haudenschild, C. D., Pradhan, S., Nelson, S. F., Pellegrini, M., & Jacobsen, S. E. (2008). Shotgun bisulphite sequencing of the Arabidopsis genome reveals DNA methylation patterning. Nature, 452(7184), 215-219.

Deniz, O., Frost, J. M., & Branco, M. R. (2019). Regulation of transposable elements by DNA modifications. Nat Rev Genet, 20(7), 417-431.

Dobin, A., Davis, C. A., Schlesinger, F., Drenkow, J., Zaleski, C., Jha, S., Batut, P., Chaisson, M., & Gingeras, T. R. (2013). STAR: ultrafast universal RNA-seq aligner. Bioinformatics, 29(1), 15-21.

Erdmann, R. M., & Picard, C. L. (2020). RNA-directed DNA Methylation. PLoS Genet, 16(10), e1009034.

Fan, M., Xu, C., Xu, K., & Hu, Y. (2012). LATERAL ORGAN BOUNDARIES DOMAIN transcription factors direct callus formation in Arabidopsis regeneration. Cell Res, 22(7), 1169-1180.

Feng, Z., Zhu, J., Du, X., & Cui, X. (2012). Effects of three auxin-inducible LBD members on lateral root formation in Arabidopsis thaliana. Planta, 236.

Frost, J. M., Kim, M. Y., Park, G. T., Hsieh, P.-H., Nakamura, M., Lin, S. J., Yoo, H., Choi, J., Ikeda, Y., & Kinoshita, T. (2018). FACT complex is required for DNA demethylation at heterochromatin during reproduction in Arabidopsis. Proc. Natl Acad. Sci. USA,

115(20), E4720-E4729.

Ge, S. X., Jung, D., & Yao, R. (2020). ShinyGO: a graphical gene-set enrichment tool for animals and plants. Bioinformatics, 36(8), 2628-2629.

Gehring, M., Bubb, K. L., & Henikoff, S. (2009). Extensive Demethylation of Repetitive Elements During Seed Development Underlies Gene Imprinting. Science, 324(5933), 1447-1451.

Gehring, M., Huh, J. H., Hsieh, T.-F., Penterman, J., Choi, Y., Harada, J. J., Goldberg, R. B., & Fischer, R. L. (2006). DEMETER DNA glycosylase establishes MEDEA polycomb gene self-imprinting by allele-specific demethylation. Cell, 124(3), 495-506.

Gehring, M., & Satyaki, P. R. (2017). Endosperm and Imprinting, Inextricably Linked. Plant Physiology, 173(1), 143-154.

Gent, J. I., Higgins, K. M., Swentowsky, K. W., Fu, F. F., Zeng, Y. B., Kim, D. W., Dawe, R. K., Springer, N. M., & Anderson, S. N. (2022). The maize gene maternal derepression of r1 encodes a DNA glycosylase that demethylates DNA and reduces siRNA expression in the endosperm. Plant Cell, 34(10), 3685-3701.

Goel, M., Sun, H., Jiao, W.-B., & Schneeberger, K. (2019). SyRI: identification of syntenic and rearranged regions from whole-genome assemblies. bioRxiv, 1.

Gordon, S. P., Heisler, M. G., Reddy, G. V., Ohno, C., Das, P., & Meyerowitz, E. M. (2007). Pattern formation during de novo assembly of the Arabidopsis shoot meristem. Development, 134.

Greenberg, M. V. C., & Bourc'his, D. (2019). The diverse roles of DNA methylation in mammalian development and disease. Nature Reviews Molecular Cell Biology, 20(10), 590-607.

Grover, J. W., Burgess, D., Kendall, T., Baten, A., Pokhrel, S., King, G. J., Meyers, B. C., Freeling, M., & Mosher, R. A. (2020). Abundant expression of maternal siRNAs is a conserved feature of seed development. Proceedings of the National Academy of Sciences of the United States of America, 117(26), 15305-15315.

Grzybkowska, D., Morończyk, J., Wójcikowska, B., & Gaj, M. D. (2018). Azacitidine (5-AzaC)-treatment and mutations in DNA methylase genes affect embryogenic response and expression of the genes that are involved in somatic embryogenesis in Arabidopsis. Plant Growth Regulation, 85, 243-256.

Gutzat, R., Rembart, K., Nussbaumer, T., Hofmann, F., Pisupati, R., Bradamante, G., Daubel, N., Gaidora, A., Lettner, N., & Donà, M.

(2020). Arabidopsis shoot stem cells display dynamic transcription and DNA methylation patterns. EMBO J., 39(20), e103667.

He, L., Zhao, C., Zhang, Q. Z., Zinta, G., Wang, D., Lozano-Durán, R., & Zhu, J. K. (2021). Pathway conversion enables a double-lock mechanism to maintain DNA methylation and genome stability. Proceedings of the National Academy of Sciences of the United States of America, 118(35).

Heard, E., & Martienssen, R. A. (2014). Transgenerational Epigenetic Inheritance: Myths and Mechanisms. Cell, 157(1), 95-109.

Hsieh, P.-H., Frost, J. M., Choi, Y., Hsieh, T.-F., Zilberman, D., & Fischer, R. L. (2023). Embryo-specific epigenetic mechanisms reconstitute the CHH methylation landscape during Arabidopsis embryogenesis. bioRxiv, 2023.2004.2006.535361.

Hsieh, P. H., He, S. B., Buttress, T., Gao, H. B., Couchman, M., Fischer, R. L., Zilberman, D., & Feng, X. Q. (2016). male sexual lineage exhibits more robust maintenance of CG methylation than somatic tissues. Proceedings of the National Academy of Sciences of the United States of America, 113(52), 15132-15137.

Hsieh, T. F., Ibarra, C. A., Silva, P., Zemach, A., Eshed-Williams, L., Fischer, R. L., & Zilberman, D. (2009). Genome-Wide Demethylation of Endosperm. Science, 324(5933), 1451-1454.

Ibarra, C. A., Feng, X., Schoft, V. K., Hsieh, T. F., Uzawa, R., Rodrigues, J. A., Zemach, A., Chumak, N., Machlicova, A., Nishimura, T., Rojas, D., Fischer, R. L., Tamaru, H., & Zilberman, D. (2012). Active DNA demethylation in plant companion cells reinforces transposon methylation in gametes. Science, 337(6100), 1360-1364.

Jeddeloh, J. A., Bender, J., & Richards, E. J. (1998). The DNA methylation locus DDM1 is required for maintenance of gene silencing in Arabidopsis. Genes & Development, 12(11), 1714-1725.

Jiang, F. W., Xu, X. F., Liu, H. L., & Zhu, J. (2015). DRM1 and DRM2 are involved in Arabidopsis callus formation. Plant Cell Tissue Organ Cult, 123.

Johnson, N. R., Yeoh, J. M., Coruh, C., & Axtell, M. J. (2016). Improved Placement of Multi-mapping Small RNAs. G3-Genes Genomes Genetics, 6(7), 2103-2111.

Jurka, J., Bao, W. D., & Kojima, K. K. (2011). Families of transposable elements, population structure and the origin of species. Biology Direct, 6.

Kankel, M. W., Ramsey, D. E., Stokes, T. L., Flowers, S. K., Haag, J. R., Jeddeloh, J. A., Riddle, N. C., Verbsky, M. L., & Richards, E. J. (2003). Arabidopsis MET1 cytosine methyltransferase mutants. Genetics, 163(3), 1109–1122.

Kareem, A., Durgaprasad, K., Sugimoto, K., Du, Y., Pulianmackal, A. J., Trivedi, Z. B., Abhayadev, P. V., Pinon, V., Meyerowitz, E. M., Scheres, B., & Prasad, K. (2015). PLETHORA genes control regeneration by a two–step mechanism. Current Biology, 25(8), 1017–1030.

Kawakatsu, T., Huang, S. S. C., Jupe, F., Sasaki, E., Schmitz, R. J., Urich, M. A., Castanon, R., Nery, J. R., Barragan, C., He, Y. P., Chen, H. M., Dubin, M., Lee, C. R., Wang, C. M., Bemm, F., Becker, C., O'Neil, R., O'Malley, R. C., Quarless, D. X.,...Consortium, G. (2016). Epigenomic Diversity in a Global Collection of Arabidopsis thaliana Accessions. Cell, 166(2), 492–505.

Kawakatsu, T., Nery, J. R., Castanon, R., & Ecker, J. R. (2017). Dynamic DNA methylation reconfiguration during seed development and germination. Genome Biology, 18.

Kim, J. Y., Yang, W., Forner, J., Lohmann, J. U., Noh, B., & Noh, Y. S. (2018). Epigenetic reprogramming by histone acetyltransferase HAG1/AtGCN5 is required for pluripotency acquisition in Arabidopsis. EMBO J., 37(20), e98726.

Kim, M. Y., Ono, A., Scholten, S., Kinoshita, T., Zilberman, D., Okamoto, T., & Fischer, R. L. (2019). DNA demethylation by ROS1a in rice vegetative cells promotes methylation in sperm. Proceedings of the National Academy of Sciences of the United States of America, 116(19), 9652–9657.

Kim, S., Park, J. S., Lee, J., Lee, K. K., Park, O. S., Choi, H. S., Seo, P. J., Cho, H. T., Frost, J. M., Fischer, R. L., & Choi, Y. (2021). The DME demethylase regulates sporophyte gene expression, cell proliferation, differentiation, and meristem resurrection. Proc Natl Acad Sci U S A, 118(29).

Lanciano, S., & Cristofari, G. (2020). Measuring and interpreting transposable element expression. Nature Reviews Genetics, 21(12), 721–736.

Lauria, M., Rupe, M., Guo, M., Kranz, E., Pirona, R., Viotti, A., & Lund, G. (2004). Extensive maternal DNA hypomethylation in the endosperm of. Plant Cell, 16(2), 510–522.

Law, J. A., & Jacobsen, S. E. (2010). Establishing, maintaining and

modifying DNA methylation patterns in plants and animals. Nature Reviews Genetics, 11(3), 204-220.

Lee, J., Lee, S., Park, K., Shin, S.-Y., Frost, J. M., Hsieh, P.-H., Shin, C., Fischer, R. L., Hsieh, T.-F., & Choi, Y. (2023). Distinct regulatory pathways contribute to dynamic CHH methylation patterns in transposable elements throughout Arabidopsis embryogenesis. Frontiers in Plant Science, 14, 1204279.

Lei, M., Zhang, H., Julian, R., Tang, K., Xie, S., & Zhu, J.-K. (2015). Regulatory link between DNA methylation and active demethylation in Arabidopsis. Proceedings of the National Academy of Sciences, 112(11), 3553-3557.

Li, B., & Dewey, C. N. (2011). RSEM: accurate transcript quantification from RNA-Seq data with or without a reference genome. BMC Bioinformatics, 12(1), 1-16.

Li, W., Liu, H., Cheng, Z. J., Su, Y. H., Han, H. N., Zhang, Y., & Zhang, X. S. (2011). DNA methylation and histone modifications regulate de novo shoot regeneration in Arabidopsis by modulating WUSCHEL expression and auxin signaling. PLoS Genet, 7.

Lin, J. Y., Le, B. H., Chen, M., Henry, K. F., Hur, J., Hsieh, T. F., Chen, P. Y., Pelletier, J. M., Pellegrini, M., Fischer, R. L., Harada, J. J., & Goldberg, R. B. (2017). Similarity between soybean and Arabidopsis seed methylomes and loss of non-CG methylation does not affect seed development. Proc Natl Acad Sci U S A, 114(45), E9730-E9739.

Lindroth, A. M., Cao, X., Jackson, J. P., Zilberman, D., McCallum, C. M., Henikoff, S., & Jacobsen, S. E. (2001). Requirement of CHROMOMETHYLASE3 for maintenance of CpXpG methylation. Science, 292(5524), 2077-2080.

Lister, R., O'Malley, R. C., Tonti-Filippini, J., Gregory, B. D., Berry, C. C., Millar, A. H., & Ecker, J. R. (2008). Highly integrated single-base resolution maps of the epigenome in Arabidopsis. Cell, 133(3), 523-536.

Liu, H., Zhang, H., Dong, Y. X., Hao, Y. J., & Zhang, X. S. (2018). DNA methyltransferase1-mediated shoot regeneration is regulated by cytokinin-induced cell cycle in Arabidopsis. New Phytol, 217.

Liu, J., Sheng, L., Xu, Y., Li, J., Yang, Z., Huang, H., & Xu, L. (2014). WOX11 and 12 are involved in the first-step cell fate transition during de novo root organogenesis in Arabidopsis. Plant Cell, 26.

Love, M. I., Huber, W., & Anders, S. (2014). Moderated estimation

of fold change and dispersion for RNA-seq data with DESeq2. Genome Biology, 15(12), 550.

Lutzmayer, S., Enugutti, B., & Nodine, M. D. (2017). Novel small RNA spike-in oligonucleotides enable absolute normalization of small RNA-Seq data. Sci Rep, 7(1), 5913.

Matzke, M. A., & Mosher, R. A. (2014). RNA-directed DNA methylation: an epigenetic pathway of increasing complexity. Nature Reviews Genetics, 15(6), 394-408.

Meng, W. J., Cheng, Z. J., Sang, Y. L., Zhang, M. M., Rong, X. F., Wang, Z. W., Tang, Y. Y., & Zhang, X. S. (2017). Type-B Arabidopsis response regulators specify the shoot stem cell niche by dual regulation of WUSCHEL. Plant Cell, 29.

Miura, A., Yonebayashi, S., Watanabe, K., Toyama, T., Shimada, H., & Kakutani, T. (2001). Mobilization of transposons by a mutation abolishing full DNA methylation in Arabidopsis. Nature, 411(6834), 212-214.

Murashige, T., & Skoog, F. (1962). A revised medium for rapid growth and bio assays with tobacco tissue cultures. Physiologia Plantarum, 15(3).

Okushima, Y., Fukaki, H., Onoda, M., Theologis, A., & Tasaka, M. (2007). ARF7 and ARF19 regulate lateral root formation via direct activation of LBD/ASL genes in Arabidopsis. Plant Cell, 19.

Ono, A., Yamaguchi, K., Fukada-Tanaka, S., Terada, R., Mitsui, T., & Iida, S. (2012). A null mutation of ROS1a for DNA demethylation in rice is not transmittable to progeny. Plant J, 71(4), 564-574.

Ortega-Galisteo, A. P., Morales-Ruiz, T., Ariza, R. R., & Roldán-Arjona, T. (2008). Arabidopsis DEMETER-LIKE proteins DML2 and DML3 are required for appropriate distribution of DNA methylation marks. Plant Molecular Biology, 67, 671-681.

Papareddy, R. K., Páldi, K., Paulraj, S., Kao, P., Lutzmayer, S., & Nodine, M. D. (2020). Chromatin regulates expression of small RNAs to help maintain transposon methylome homeostasis in Arabidopsis. Genome Biology, 21, 1-24.

Park, K., Kim, M. Y., Vickers, M., Park, J. S., Hyun, Y., Okamoto, T., Zilberman, D., Fischer, R. L., Feng, X., Choi, Y., & Scholten, S. (2016). DNA demethylation is initiated in the central cells of Arabidopsis and rice. Proc Natl Acad Sci U S A, 113(52), 15138-15143.

Penterman, J., Zilberman, D., Huh, J. H., Ballinger, T., Henikoff, S., & Fischer, R. L. (2007). DNA demethylation in the Arabidopsis genome.

Proc Natl Acad Sci USA, 104.

Picard, C. L., & Gehring, M. (2017). Proximal methylation features associated with nonrandom changes in gene body methylation. Genome Biol, 18(1), 73.

Plotnikova, A., Kellner, M. J., Schon, M. A., Mosiolek, M., & Nodine, M. D. (2019). MicroRNA Dynamics and Functions During Arabidopsis Embryogenesis. Plant Cell, 31(12), 2929-2946.

Quadrana, L., Bortolini Silveira, A., Mayhew, G. F., LeBlanc, C., Martienssen, R. A., Jeddeloh, J. A., & Colot, V. (2016). The Arabidopsis thaliana mobilome and its impact at the species level. Elife, 5.

Quesneville, H. (2020). Twenty years of transposable element analysis in the Arabidopsis thaliana genome. Mob DNA, 11, 28.

Rajkumar, M. S., Gupta, K., Khemka, N. K., Garg, R., & Jain, M. (2020). DNA methylation reprogramming during seed development and its functional relevance in seed size/weight determination in chickpea. Communications Biology, 3(1).

Raju, S. K. K., Ritter, E. J., & Niederhuth, C. E. (2019). Establishment, maintenance, and biological roles of non-CG methylation in plants. DNA Methylation, 63(6), 743-755.

Rashotte, A. M., Mason, M. G., Hutchison, C. E., Ferreira, F. J., Schaller, G. E., & Kieber, J. J. (2006). A subset of Arabidopsis AP2 transcription factors mediates cytokinin responses in concert with a two-component pathway. Proc. Natl Acad. Sci. USA, 103(29), 11081-11085.

Reik, W. (2007). Stability and flexibility of epigenetic gene regulation in mammalian development. Nature, 447(7143), 425-432.

Sasaki, H., & Matsui, Y. (2008). Epigenetic events in mammalian germ-cell development: reprogramming and beyond. Nature Reviews Genetics, 9(2), 129-140.

Schoft, V. K., Chumak, N., Choi, Y., Hannon, M., Garcia-Aguilar, M., Machlicova, A., Slusarz, L., Mosiolek, M., Park, J. S., Park, G. T., Fischer, R. L., & Tamaru, H. (2011). Function of the DEMETER DNA glycosylase in the Arabidopsis thaliana male gametophyte. Proc. Natl Acad. Sci. USA, 108(19), 8042-8047.

Seisenberger, S., Peat, J. R., Hore, T. A., Santos, F., Dean, W., & Reik, W. (2013). Reprogramming DNA methylation in the mammalian life cycle: building and breaking epigenetic barriers. Philosophical Transactions of the Royal Society B-Biological Sciences, 368(1609).

Seki, Y., Hayashi, K., Itoh, K., Mizugaki, M., Saitou, M., & Matsui, Y. (2005). Extensive and orderly reprogramming of genome-wide chromatin modifications associated with specification and early development of germ cells in mice. Developmental Biology, 278(2), 440-458.

Shemer, O., Landau, U., Candela, H., Zemach, A., & Williams, L. E. (2015). Competency for shoot regeneration from Arabidopsis root explants is regulated by DNA methylation. Plant Sci, 238.

Shim, S., Lee, H. G., Park, O. S., Shin, H., Lee, K., Lee, H., Huh, J. H., & Seo, P. J. (2021). Dynamic changes in DNA methylation occur in TE regions and affect cell proliferation during leaf-to-callus transition in Arabidopsis. Epigenetics, 15.

Shim, S., Lee, H. G., & Seo, P. J. (2021). MET1-dependent DNA methylation represses light signaling and influences plant regeneration in Arabidopsis. Mol Cells, 44.

Sigman, M. J., & Slotkin, R. K. (2016). The First Rule of Plant Transposable Element Silencing: Location, Location, Location. Plant Cell, 28(2), 304-313.

Skoog, F., & Miller, C. O. (1957). Chemical regulation of growth and organ formation in plant tissues cultured in vitro. Symp Soc Exp Biol, 11.

Stroud, H., Ding, B., Simon, S. A., Feng, S., Bellizzi, M., Pellegrini, M., Wang, G. L., Meyers, B. C., & Jacobsen, S. E. (2013). Plants regenerated from tissue culture contain stable epigenome changes in rice. Elife, 2, e00354.

Stroud, H., Greenberg, M. V. C., Feng, S. H., Bernatavichute, Y. V., & Jacobsen, S. E. (2013). Comprehensive Analysis of Silencing Mutants Reveals Complex Regulation of the Methylome. Cell, 152(1-2), 352-364.

Sugimoto, K., Jiao, Y., & Meyerowitz, E. M. (2010). Arabidopsis regeneration from multiple tissues occurs via a root development pathway. Dev Cell, 18.

Surani, M. A., Hayashi, K., & Hajkova, P. (2007). Genetic and epigenetic regulators of pluripotency. Cell, 128(4), 747-762.

Turker, M. S. (2002). Gene silencing in mammalian cells and the spread of DNA methylation. Oncogene, 21(35), 5388-5393.

Williams, B. P., Pignatta, D., Henikoff, S., & Gehring, M. (2015). Methylation-Sensitive Expression of a DNA Demethylase Gene Serves As an Epigenetic Rheostat. PLOS Genetics, 11(3), e1005142.

Xing, M. Q., Zhang, Y. J., Zhou, S. R., Hu, W. Y., Wu, X. T., Ye, Y. J., Wu, X. X., Xiao, Y. P., Li, X., & Xue, H. W. (2015). Global Analysis Reveals the Crucial Roles of DNA Methylation during Rice Seed Development. Plant Physiology, 168(4), 1417-U1554.

Xu, Q., Wu, L. M., Luo, Z. X., Zhang, M., Lai, J. S., Li, L., Springer, N. M., & Li, Q. (2022). DNA demethylation affects imprinted gene expression in maize endosperm. Genome Biology, 23(1).

Xu, W., Yang, T. Q., Dong, X., Li, D. Z., & Liu, A. Z. (2016). Genomic DNA Methylation Analyses Reveal the Distinct Profiles in Castor Bean Seeds with Persistent Endosperms. Plant Physiology, 171(2), 1242-1258.

Yanai, O., Shani, E., Dolezal, K., Tarkowski, P., Sablowski, R., Sandberg, G., Samach, A., & Ori, N. (2005). Arabidopsis KNOXI proteins activate cytokinin biosynthesis. Current Biology, 15(17), 1566-1571.

Yelagandula, R., Stroud, H., Holec, S., Zhou, K., Feng, S. H., Zhong, X. H., Muthurajan, U. M., Nie, X., Kawashima, T., Groth, M., Luger, K., Jacobsen, S. E., & Berger, F. (2014). The Histone Variant H2A. W Defines Heterochromatin and Promotes Chromatin Condensation in. Cell, 158(1), 98-109.

Yoo, H., Park, K., Lee, J., Lee, S., & Choi, Y. (2021). An Optimized Method for the Construction of a DNA Methylome from Small Quantities of Tissue or Purified DNA from Arabidopsis Embryo. Molecules and Cells, 44(8), 602-612.

Zemach, A., Kim, M. Y., Hsieh, P. H., Coleman-Derr, D., Eshed-Williams, L., Thao, K., Harmer, S. L., & Zilberman, D. (2013). The Arabidopsis nucleosome remodeler DDM1 allows DNA methyltransferases to access H1-containing heterochromatin. Cell, 153(1), 193-205.

Zemach, A., Kim, M. Y., Silva, P., Rodrigues, J. A., Dotson, B., Brooks, M. D., & Zilberman, D. (2010). Local DNA hypomethylation activates genes in rice endosperm. Proc Natl Acad Sci U S A, 107(43), 18729-18734.

Zhang, A., Matsuoka, K., Kareem, A., Robert, M., Roszak, P., Blob, B., Bisht, A., De Veylder, L., Voiniciuc, C., & Asahina, M. (2022). Cell-wall damage activates DOF transcription factors to promote wound healing and tissue regeneration in Arabidopsis thaliana. Current Biology, 32(9), 1883-1894. e1887.

Zhang, T. Q., Lian, H., Zhou, C. M., Xu, L., Jiao, Y., & Wang, J. W.

(2017). A two-step model for de novo activation of WUSCHEL during plant shoot regeneration. The Plant Cell, 29(5), 1073-1087.

Zhao, S., Cheng, L., Gao, Y., Zhang, B., Zheng, X., Wang, L., Li, P., Sun, Q., & Li, H. (2019). Plant HP1 protein ADCP1 links multivalent H3K9 methylation readout to heterochromatin formation. Cell Res, 29(1), 54-66.

Zilberman, D., Gehring, M., Tran, R. K., Ballinger, T., & Henikoff, S. (2007). Genome-wide analysis of Arabidopsis thaliana DNA methylation uncovers an interdependence between methylation and transcription. Nature Genetics, 39(1), 61-69.

Ziller, M. J., Hansen, K. D., Meissner, A., & Aryee, M. J. (2015). Coverage recommendations for methylation analysis by whole-genome bisulfite sequencing. Nat Methods, 12(3), 230-232, 231 p following 232.

Abstract in Korean

식물의 재분화 과정과 배 발달 과정 동안에는 공통적으로 DNA 메틸화에 의한 동적인 에피유전학적 재프로그래밍이 나타난다. 본 연구는 애기장대를 대상으로 전장 유전체 이황화 시퀀싱(WGBS), RNA 시퀀싱, 그리고 소형 RNA(sRNA) 프로파일링을 활용하여 이러한 과정의 복잡한 에피유전학적 다이나믹스를 규명하였다. 식물 재분화 과정에서 분화된 잎 조직이 전능성을 가지는 캘러스로 전환되고 최종적으로 새싹이 형성되는 동안 DNA 메틸화 패턴의 광범위한 재프로그래밍이 일어난다. 캘러스 형성 단계에서 중심체 주변부의 전이인자(TE) 영역은 주로 CHH 맥락(H는 A, T, C를 나타냄)에서, 그리고 일부 CG 맥락에서 탈메틸화가 일어나며, 유전자 영역에서는 세포 재프로그래밍을 가능하게 하는 CG 메틸화의 재분배가 나타난다. 이어지는 새싹 재분화 단계에서는 중심체 주변부 TE에서 모든 사이토신 맥락의 광범위한 메틸화와 유전자 영역에서의 동적인 CG 메틸화 변화가 특징적이다. 이러한 에피유전학적 변화는 DEMETER(DME) DNA 탈메틸화효소에 의해 중요하게 조절되며, 이 과정에서 DME는 ROS1 및 RNA 의존적 DNA 메틸화(RdDM) 경로와 상호작용하여 메틸화 균형을 유지한다. DME 돌연변이는 메틸화 패턴의 변화와 캘러스 및 새싹 재분화의 증가를 초래하며, 이는 재분화 과정에서 TE 활성화와 유전체 불안정성에 대한 에피유전학적 안전장치로서의 역할을 강조한다. 배 발달 과정에서는 CHH 메틸화 수준이 점진적으로 증가하며, 이는 RdDM과 RNA 비의존적인 CHROMOMETHYLASE 2(CMT2) 경로를 모두 포함한다. 이 과정은 TE에서의 두 단계의 발달적 sRNA 축적을 특징으로 하며, CHH 메틸화 영역과 sRNA 클러스터의 동반 확장을 유도한다. CHH 메틸화는 sRNA 의존적인 연속 메틸화 부위의 연장과 sRNA 비의존적 기작을 통해 확산되며, 특히 중심체 영역에서 두드러진다. 이러한 발견은 발달 가소성과 유전체 안정성을 조절하는 DNA 메틸화 다이나믹스의 보존된 원리를 강조한다. 식물의 CG

메틸화는 상대적으로 안정적인 반면, 식물 재분화와 배 발달 과정에서 관찰되는 CHH 메틸화의 재설정은 포유류 배아 발생 중 CG 메틸화 다이나믹스와 유사한 패턴을 보인다. 이 비교 분석은 세포 운명 전환을 조절하는 맥락 특이 에피유전학적 전략에 대한 중요한 통찰을 제공하며, 식물 재분화 효율성을 조작하고 에피유전학적 조절의 진화적 보존을 이해하기 위한 프레임워크를 제시한다. 종합적으로, 본 연구는 식물 발달 생물학에 대한 이해를 증진시키고, 식물 육종을 위한 조직 배양 기술 향상과 생명공학적 조작 과정에서 유전체 안정성을 유지하기 위한 전략 개발 등 작물 개량에 잠재적 응용 가능성을 제시한다.

주요어: DNA 메틸레이션, 에피유전학, 식물재분화, 배발생, DEMETER 탈메틸화효소, 애기장대
학번: 2017-28950